AIMS Mathematics, 10(8): 18731–18769.
DOI: 10.3934/math.2025837
Received: 18 June 2025
Revised: 02 August 2025
Accepted: 05 August 2025
Published: 19 August 2025

https://www.aimspress.com/journal/Math

Research article

A novel extension to the unit Weibull distribution: properties and inference with applications to medicine, engineering, and radiation

Hassan Eid Elghaly[1,2,*], Mohamed A. Abd Elgawad[3] and Boping Tian[1,*]

[1] School of Mathematics, Harbin Institute of Technology, Harbin 150001, China
[2] Department of Applied Statistics and Insurance, Faculty of Commerce, Mansoura University, Mansoura 35516, Egypt
[3] Department of Mathematics and Statistics, College of Science, Imam Mohammad Ibn Saud Islamic University (IMSIU), Riyadh 11432, Saudi Arabia; moaasalem@imamu.edu.sa

* **Correspondence:** Email: hassanghaly@mans.edu.eg, bopingt361147@hit.edu.cn.

Abstract: This study introduces a new extension of the unit Weibull distribution called the unit power generalized Weibull distribution (UPGWD). The UPGWD arises from inverse exponential function transformation of the power generalized Weibull distribution. It is a highly competitive distribution compared with the existing unit distributions in the literature, offering significant flexibility. The probability density function of the UPGWD can display several forms, including constant, bathtub, unimodal, J-shaped (increasing), and inverted J-shaped (decreasing) configurations. Conversely, its hazard function may exhibit increasing J-shaped and bathtub configurations. Some of its corresponding basic statistical and reliability properties are introduced. Furthermore, the maximum likelihood estimation (MLE) technique is applied to estimate its parameters. A Monte Carlo simulation study is performed to assess the accuracy of the MLE estimates. Finally, to demonstrate the potential importance of the UPGWD, four applications with actual lifetime data related to COVID-19, reliability, engineering, and radiation are discussed. The empirical application further validated its efficacy, surpassing the earlier existing unit Weibull distributions, including the unit Weibull, the unit inverted exponentiated Weibull, the upper truncated Weibull, the bounded exponentiated Weibull, the power upper truncated Weibull, and the Poisson unit Weibull distributions.

Keywords: Weibull distribution; unit distributions; reliability; survival function; bathtub-shaped; stress–strength reliability; maximum likelihood estimation; Monte Carlo simulation
Mathematics Subject Classification: 60E05, 62G05, 62N05

1. Introduction

Professionals in diverse fields of life sciences, including biomedical sciences, engineering, economics, and medicine, as well as reliability studies, continually confront complex real-world phenomena. The primary challenge faced by those is to identify the patterns of these phenomena. Probability distributions play a crucial role in analyzing real-life data in various areas of applied science [1]. However, when it comes to modeling and describing such phenomena, an essential challenge arises in choosing a distribution that provides an adequate fit to the data [2]. In many practical scenarios, the classical existing distributions often do not accurately represent the phenomena [3]. This case therefore underlines the need for novel probability distributions. That is why statisticians have recently introduced new families of probability models that can provide a satisfactory fit to real-world data by adding an extra parameter or more to the existing classical models.

On the other hand, in many practical studies, the data of a particular phenomenon is defined in a (0, 1) domain, such as mortality rates, proportions, and percentages that are often detected in risk management and insurance, income analysis, industry applications, economics, the biological and medical sectors, hydrology, and demography, to name a few [4]. For instance, in demographics, we possess data on sex, dependency, abortion, and child–woman ratios that can be used; in economics, we have the proportion of family income allocated to food, along with notable ratios such as money saved to revenue, capital to output, labor's share of income, revenue's speed of circulation, the ratio of defaults on loans, and capital to work ratios. In environmental studies, examples include the percentage of forest areas affected by logging and the ratio of water purity parameters that exceed safety thresholds. In psychology, percentages and proportions are valuable for assessing possible consequences, such as the percentage of cognitive processes influenced by a specific location. In engineering and associated disciplines, we encounter the aspect ratio in aeronautics and the fineness ratio in marine architecture and aerospace engineering, as well as statistics that often relate to the effectiveness of solar energy systems and the percentage of waste that is filtered and reused. In public health, metrics quantifying the recovery rate from COVID-19 and indicators for vaccine efficacy illustrate the management of health outcomes within population constraints [4,5]. The most familiar unit model used to model such bounded data is the two-parameter beta distribution [6]. The beta distribution is the most widely used double-bounded distribution for modeling data ranging from 0 to 1. However, this suffers from some limitations regarding its nonclosed-form cumulative distribution function (CDF) and quantile function (QF), which constrain the use of the beta distribution in most applications.

As a result, authors have been drawn to the idea of creating and offering novel probability distributions that can provide models that fit datasets defined on the (0, 1) domain, featuring appealing representations for the CDF and QF and a range of forms of the hazard rate functions (HRF). The authors in [7] presented a new bounded distribution known as the Topp–Leone distribution. Another practical unit interval model is the Kumaraswamy distribution, derived by [3]. It is similar to the beta distribution and is used as an analogous and well-recognized alternative due to its simplicity and familiarity. In contrast to the CDF of the beta distribution, the CDF of the Kumaraswamy distribution is more manageable to utilize. In addition to the Kumaraswamy distribution, several alternative unit distributions have emerged to reflect the increasing array of datasets on the unit interval, which may originate from various complex events, with the primary objective of enhancing the fit capabilities for such data. Most of these distributions have been generated using an inevitable transformation and

different modification strategies on any one of the parent distributions, and have been made available for application in lifetime dataset modeling and statistical analysis [8,9].

Various significant contributions are included in the literature, including the unit gamma distribution by [10,11], was derived by using the transformations $V = e^{-T}$, where $T\sim$ is the gamma distribution. The two-parameter log-Lindley and the one-parameter unit Lindley distributions are presented in [12,13], respectively. Following the same previous logarithmic transformation of the Birnbaum–Saunders distribution, the unit Birnbaum–Saunders distribution has been derived by [14], and the unit Gompertz distribution has been defined by [15]. Apart from those models, noteworthy contributions have applied the same technique and other different variable transformations, introducing bounded distributions such as the unit inverse Gaussian distribution by [16], the unit half logistic geometric distribution by [17], the unit Rayleigh distribution by [18], the unit Nadarajah and Haghighi distribution by [19], the unit generalized log Burr XII distribution [20], the unit folded normal distribution [21], the unit power Burr X distribution by [2], and the generalized unit Weibull distribution [22]. For further examples of other practical unit models, please refer to [2,22,23].

The Weibull distribution [24] is renowned as the predominant model for lifetime analysis and has been extensively utilized in engineering, reliability, and biological research over recent decades. Due to their simplicity and adaptability, the Weibull and exponentiated Weibull models are often applied in survival analysis. Using the Weibull distribution and the exponentiated distribution as a base, several important unit distributions have been recently created through different variable changes, such as the unit Weibull distribution (UWD) [8], the unit inverted exponentiated Weibull distribution (UIEWD) [25], the upper truncated Weibull distribution (UTWD) [4], the bounded exponentiated Weibull distribution (BEWD) [5], the power upper truncated Weibull distribution (PUTWD) [26], and the Poisson unit Weibull distribution (PUWD) [1]. Despite these advancements and contributions to unit distributions, most still exhibit some limitations, particularly regarding restricted tail behavior and challenges in deriving specific statistical properties. These limitations include the following. (a) Most existing models possess only two parameters, which may be insufficient for capturing the complexity of intricate datasets, especially those related to sophisticated phenomena such as hydro-environmental data. (b) The probability density function (PDF) and CDF of some distributions cannot be expressed in simple closed forms, complicating the derivation of various mathematical and reliability properties. (c) Some unit distributions also lack a closed-form QF, further limiting their analytical tractability. To overcome these limitations, this study presents an innovative, flexible extension of the UW distribution, as detailed in Section 2. This new extension significantly enhances the flexibility and applicability of the UW distribution, enabling it to model a broader spectrum of real-world scenarios. This latest extension addresses a significant void in the current statistical literature. Numerous fundamental factors drove the creation of the suggested model. Its PDF can display several forms, including the constant, bathtub, unimodal, J-shaped (increasing), and inverted J-shaped (decreasing) configurations. At the same time, its hazard function may exhibit increasing, J-shaped, and bathtub configurations. Such versatility allows the model to encompass many data patterns. The detailed derivation of the model's essential features, such as moments, quantile function, and order statistics, offers a sophisticated theoretical comprehension. These features make the model a significant asset for many applications. Moreover, utilizing the maximum likelihood estimation (MLE) approach for parameter estimation guarantees the model's flexibility across diverse estimation methodologies. A thorough simulation analysis validated the consistency of the MLE, enhancing trust in the model's dependability for practical applications. The successful application of the suggested model to four real-world datasets

further validated its efficacy, surpassing the abovementioned existing unit Weibull distributions. The inclusion of our proposed model significantly enriches the statistical literature, offering academics and practitioners a diverse instrument for improved analysis and understanding of data.

The remainder of this study is organized as follows: Section 2 discusses the proposed model formulation. Section 3 presents some reliability metrics for the model. We examine its associated statistical features in Section 4. Some additional aspects of the UPGWD, including the mean deviations, inequality measures (Lorenz and Bonferroni curves), and order statistics, are studied in Section 5. In Section 6, we employ the MLE method to ascertain its parameters. In Section 7, we perform a Monte Carlo simulation analysis to assess the precision of the MLE. Section 8 offers four applications utilizing actual lifetime data to illustrate the potential impact of our suggested distribution. The final section concludes our study.

2. The proposed distribution formulation

Dimitrakopoulou et al. [27] presented a very flexible generalization of the well-known Weibull distribution with three parameters, named the power generalized Weibull distribution (PGWD). Its CDF is given by

$$G(t;\boldsymbol{\theta}) = 1 - e^{1-(1+\lambda t^{\alpha})^{\beta}}, \tag{2.1}$$

for $t > 0$, with $\boldsymbol{\theta} = (\alpha, \beta, \lambda)$, where $\alpha, \beta > 0$ are shape parameters and $\lambda > 0$ is a scale parameter. Its PDF is as follows:

$$g(t;\boldsymbol{\theta}) = \alpha\beta\lambda t^{\alpha-1}(1+\lambda t^{\alpha})^{\beta-1} e^{1-(1+\lambda t^{\alpha})^{\beta}}. \tag{2.2}$$

Here, we propose the novel unit power generalized Weibull distribution by using the same convolution technique of [2,8,10,14,15], referred to as the UPGWD. By using the logarithmic transformation $V = e^{-T}$, where T follows the PGWD in (2.1), the CDF of the UPGWD can be derived.

Proposition 2.1. *If T is a random variable PGWD with (2.1), then a random variable $V = e^{-T}$~UPGWD with $F(v;\boldsymbol{\theta}) = 1 - G_T(-\ln v\,;\boldsymbol{\theta})$.*

Proof. $F(v{:}\,\boldsymbol{\theta}) = P(V \le v) = P(e^{-T} \le v) = P(-T \le \ln v) = 1 - P(T \le -\ln v) = 1 - G_T(-\ln v\,;\boldsymbol{\theta})$.

Therefore, we derive the CDF of the UPGWD as follows:

$$F(v;\boldsymbol{\theta}) = e^{1-(1+\lambda(-\ln v)^{\alpha})^{\beta}}, v \in (0,1),\ \alpha,\beta,\lambda > 0. \tag{2.3}$$

We have $F(v;\boldsymbol{\theta}) = 0$ for $v \le 0$, and $F(v;\boldsymbol{\theta}) = 1$ for $v \ge 1$.

Proposition 2.2. $F(v;\boldsymbol{\theta})$ *is increasing* $\forall v \in (0,1)$.

Proof. First, by taking the natural logarithm of $F(v;\boldsymbol{\theta})$,

$$\ln F(v;\theta) = 1 - (1+\lambda(-\ln v)^{\alpha})^{\beta}.$$

Now, we differentiate both sides with respect to v

$$\frac{F'(v;\boldsymbol{\theta})}{F(v;\boldsymbol{\theta})} = -\beta(1+\lambda(-ln\ v)^{\alpha})^{\beta-1}.\left(\frac{-\alpha\lambda}{v}(-ln\ v)^{\alpha-1}\right).$$

Simplify the following:

$$F'(v;\boldsymbol{\theta}) = F(v;\boldsymbol{\theta}).\frac{\alpha\beta\lambda}{v}(-ln\ v)^{\alpha-1}(1+\lambda(-ln\ v)^{\alpha})^{\beta-1}.$$

We now verify that every term in $F'(v;\boldsymbol{\theta})$ *is strictly positive for* $v \in (0,1)$. *Since* $(1+\lambda(-ln\ v)^{\alpha})^{\beta} > 1$ *because* $\alpha,\beta,\lambda > 0$, *and*$(-ln\ v) > 0$ *for* $v \in (0,1)$, *it follows that* $F(v;\boldsymbol{\theta}) > 0$. *The term* $(-ln\ v)^{\alpha-1} > 0$ *since* $(-ln\ v) > 0$ *for* $v \in (0,1)$ *and* $\alpha > 0$*; even if* $\alpha - 1 < 0$, *a positive number raised to any real power remains positive. Moreover,* $1/v > 0$ *for* $v \in (0,1)$, $(1+\lambda(-ln\ v)^{\alpha})^{\beta-1} > 1$, *and* $\beta > 0$*; the term is strictly positive, i.e., all factors in* $F'(v;\boldsymbol{\theta})$ *are positive. Therefore,* $F(v;\boldsymbol{\theta})$ *is increasing. Thus defined,* $F(v;\boldsymbol{\theta})$ *has the required properties of a continuous CDF, and the UPGWD's PDF is defined as follows:*

$$f(v;\boldsymbol{\theta}) = \frac{\alpha\beta\lambda}{v}(-ln\ v)^{\alpha-1}(1+\lambda(-ln\ v)^{\alpha})^{\beta-1}e^{1-(1+\lambda(-ln\ v)^{\alpha})^{\beta}}. \tag{2.4}$$

To the best of our knowledge, the CDF presented in (2.3) has never been introduced in the literature, and we contribute to the existing literature by introducing the UPGWD in several key ways:

(1) One of the most notable features of this new UPGWD is its flexibility. Its PDF (2.4) can display several forms, including constant, bathtub (U-shaped), unimodal, J-shaped (increasing), and inverted J-shaped (decreasing) configurations (refer to Figure 1).

(2) Its HRFs may exhibit increasing, J-shaped, and bathtub (U-shaped) configurations (refer to Figure 1), which can be very useful and valuable for modeling data related to the medical sector, reliability engineering, and other practical domains.

(3) Its CDF (2.3) can be reduced to five well-known distributions as submodels by assigning different values to subsets of its parameters; see Table 1.

(4) Unlike the beta distribution, it has a closed form for its PDF and CDF, making it easier to derive several of its statistical and reliability properties than other classical distributions.

(5) Its QF also has a closed-form expression, which is helpful for many simulations and hydrology applications, generating pseudo-random numbers and introducing a quantile regression model.

(6) Its three shape parameters have provided additional flexibility in modeling heavy-tailed or highly skewed data compared with other existing UWDs. That is, it offers more control over all common types of data, whether left-skewed, positively skewed, platykurtic, leptokurtic, and mesokurtic data, as will be discussed later.

(7) The detailed derivation of the model's essential properties, including moments, inequality measures, and order statistics, provides a sophisticated theoretical understanding of the model.

(8) The empirical application for modeling four real-world datasets further validated its efficacy, surpassing the abovementioned existing UWDs, including the UWD, the PUWD, the PUTWD, the UTWD, the BEWD, and the UIEWD.

Table 1. Special submodels of the UPGWD.

α	β	λ	Distribution	Author(s)
1	-	-	Unit Nadarajah and Haghighi	[19]
-	1	-	Unit Weibull	[8]
2	1	-	Unit Rayleigh	[18]
1	1	-	Lehman Type I or Power function Type I	[28,29]
1	1	1	Standard uniform	[28,29]

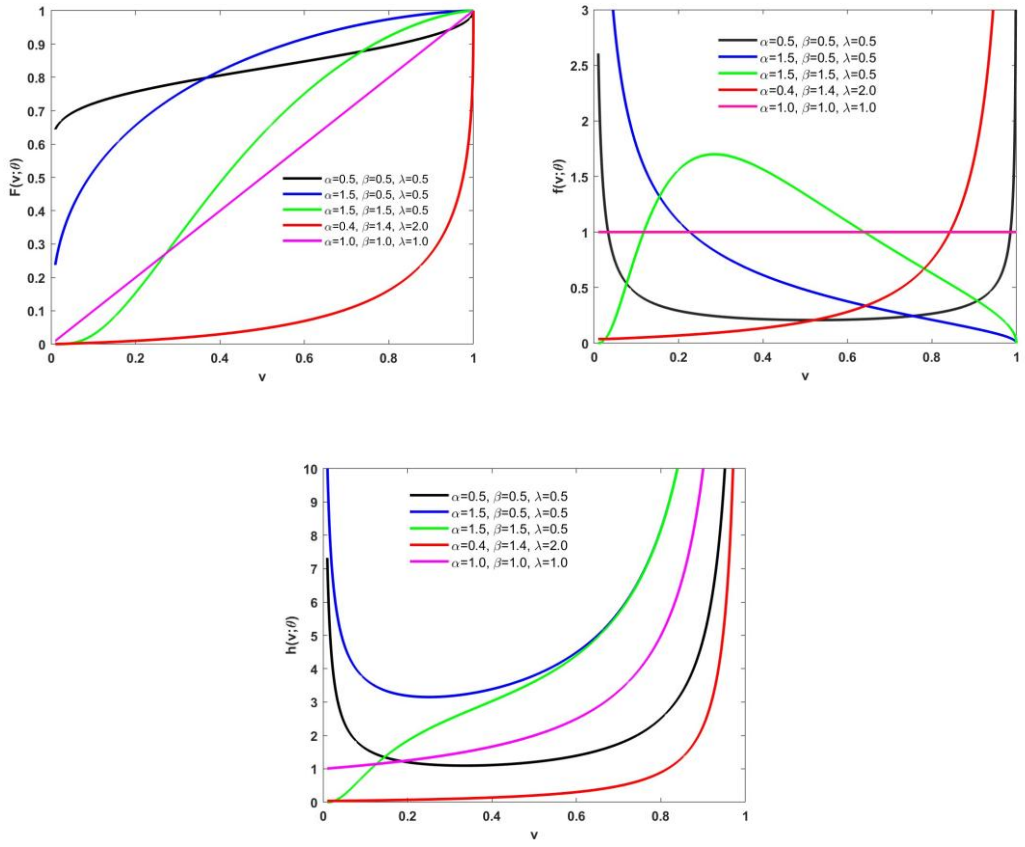

Figure 1. Plots of the UPGWD's CDF, PDF, and HRF for selected values of α, β, and λ.

3. Some reliability measures

Here, we discuss some reliability measures for the UPGWD, which are useful tools in engineering, reliability, actuarial science, economics, survival analysis, and demography.

3.1. The reliability (survival) function

One of the most widely used tools in survival analysis, engineering, and lifetime assessments is the survival function, which estimates the likelihood that a product will continue to function without failure for a particular duration [4]. The survival function (SF) of the UPGWD can be given by

$$R(v;\boldsymbol{\theta}) = P(V > v) = 1 - F(v;\boldsymbol{\theta}) = 1 - e^{1-(1+\lambda(-\ln v)^{\alpha})^{\beta}}, 0 < v < 1. \quad (3.1)$$

3.2. The hazard rate function

A further crucial component of survival analysis is the HRF. It represents the chance that if a certain event survives until time t, it will also survive until the subsequent time $t + \varepsilon$. This is the conditional chance of survival, contingent upon the event of interest not having occurred before time t [30]. It may be expressed mathematically as [31]

$$h(v;\boldsymbol{\theta}) = \frac{f(v;\boldsymbol{\theta})}{S(v;\boldsymbol{\theta})} = \frac{\alpha\beta\lambda\,(-ln\ v)^{\alpha-1}(1+\lambda(-ln\ v)^{\alpha})^{\beta-1}e^{1-(1+\lambda(-ln\ v)^{\alpha})^{\beta}}}{v\left(1-e^{1-(1+\lambda(-ln\ v)^{\alpha})^{\beta}}\right)}, 0 < v < 1. \tag{3.2}$$

A notable strength and impetus for introducing the UPGWD are the bathtub and J-shaped characteristics of its HRF. This flat region of the J-shaped HRF, referred to as the long applicable period, is critical and is arguably one of the most significant phases for prediction and evaluation of reliability, as it delineates the normal lifespan of the component or system. Consequently, possessing a model that can effectively capture this flat region is paramount. Our model is adept at modeling both the long useful and the final (wear-out) phases of various lifetime phenomena, with wear-out periods typically resulting from the natural accumulation of detrimental effects.

3.3. The reverse hazard rate function

Alongside $S(v;\boldsymbol{\theta})$ and the HRF, the reverse HRF is also a significant metric of reliability. It is mathematically expressed as

$$rh(v;\boldsymbol{\theta}) = \frac{f(v;\boldsymbol{\theta})}{F(v;\boldsymbol{\theta})} = \frac{\alpha\beta\lambda}{v}(-ln\ v)^{\alpha-1}(1+\lambda(-ln\ v)^{\alpha})^{\beta-1}. \tag{3.3}$$

The authors of [32] have shown that although the latter function is utilized less frequently than the HRF, it serves as an effective metric for evaluating concealed failures, waiting periods, and periods of inactivity. In addition to its application in reliability engineering for system analysis, replacement methods, and maintenance, it serves as a valuable instrument in actuarial science, medicine, and the study of left-censored and right-truncated data.

3.4. The odds function

Another significant metric of reliability is the odds ratio. It has been utilized in reliability engineering and survival analysis. It may be characterized as the ratio of the cumulative distribution function to the survival function.

$$O(v;\boldsymbol{\theta}) = \frac{F(v;\boldsymbol{\theta})}{S(v;\boldsymbol{\theta})} = \frac{1}{S(v;\boldsymbol{\theta})} - 1 = \left[1 - e^{1-(1+\lambda(-ln\ v)^{\alpha})^{\beta}}\right]^{-1} - 1. \tag{3.4}$$

It should be noted that the HRF (3.2) can be defined as the product of Eqs (3.3) and (3.4).

3.5. The Mills ratio

The result of dividing (3.1) by (2.4) is referred to as the Mills ratio. It serves as an additional reliability metric alongside the preceding four functions and may be mathematically articulated as the reciprocal of the HRF as follows:

$$M(v;\theta) = \frac{S(v;\boldsymbol{\theta})}{f(v;\boldsymbol{\theta})} = \frac{v\left(1-e^{1-(1+\lambda(-\ln\ v)^{\alpha})^{\beta}}\right)}{\alpha\beta\lambda\,(-\ln\ v)^{\alpha-1}(1+\lambda(-\ln\ v)^{\alpha})^{\beta-1}e^{1-(1+\lambda(-\ln\ v)^{\alpha})^{\beta}}}, 0 < v < 1. \tag{3.5}$$

While these functions were first introduced in the actuarial literature, they are commonly applied in survival analysis, providing statisticians with supplementary tools to evaluate the consequences of using a particular distribution and uncover model attributes that are otherwise difficult to discern. The HRF is the most commonly used among the preceding functions.

3.6. Stress–strength reliability coefficient

The stress–strength reliability (SSR) coefficient is an invaluable metric for assessing the performance of a system or component. It is used to measure the probability that a specific system or component with a random strength V_1 and subjected to a random stress V_2 will not fall short, denoted as $R = P(V_2 < V_1)$. Otherwise, the system will collapse if the random stress V_2 exceeds its strength V_1 [33]. It is extensively used in physics, biostatistics, and reliability engineering, such as the decline of rocket engines and the aging of concrete vessels [34]. Suppose that V_1 has the UPGWD $(\alpha, \beta_1, \lambda)$ and V_2 has the UPGWD $(\alpha, \beta_2, \lambda)$, where both are independent random variables. The SSR then may be obtained as follows:

$$R = P(V_2 < V_1) = \int_0^1 f_{V_1}(v)F_{V_2}(v)dv. \tag{3.6}$$

By using the CDF (2.3) and PDF (2.4), we have the following:

$$R = \int_0^1 \frac{\alpha\beta_1\lambda}{v}(-\ln\ v)^{\alpha-1}(1+\lambda(-\ln\ v)^{\alpha})^{\beta_1-1}e^{1-(1+\lambda(-\ln\ v)^{\alpha})^{\beta_1}}e^{1-(1+\lambda(-\ln\ v)^{\alpha})^{\beta_2}}\,dv$$

$$= \int_0^1 \frac{\alpha\beta_1\lambda}{v}(-\ln\ v)^{\alpha-1}(1+\lambda(-\ln\ v)^{\alpha})^{\beta_1-1}e^{2-(1+\lambda(-\ln\ v)^{\alpha})^{\beta_1}-(1+\lambda(-\ln\ v)^{\alpha})^{\beta_2}}dv. \tag{3.7}$$

By setting $t = 1+\lambda(-\ln\ v)^{\alpha}$, the integral can be written as

$$R = \beta_1\int_1^{\infty} t^{\beta_1-1}e^{2-t^{\beta_1}-t^{\beta_2}}dt = \beta_1 e^2\int_1^{\infty} t^{\beta_1-1}e^{-t^{\beta_1}}e^{-t^{\beta_2}}dt. \tag{3.8}$$

By using the exponential series [35], we have

$$e^{-t^{\beta_2}} = \sum_{n=0}^{\infty}\frac{(-1)^n t^{n\beta_2}}{n!}.$$

Thus, the integral becomes

$$R = \beta_1 e^2 \sum_{n=0}^{\infty} \frac{(-1)^n}{n!} \int_1^{\infty} t^{\beta_1 + n\beta_2 - 1} e^{-t^{\beta_1}} dt. \tag{3.9}$$

By setting $z = t^{\beta_1}$, the integral could potentially be expressed in terms of the upper incomplete gamma function as follows:

$$R = e^2 \sum_{n=0}^{\infty} \frac{(-1)^n}{n!} \int_1^{\infty} z^{\frac{n\beta_2}{\beta_1}} e^{-z} dz, \tag{3.10}$$

where $\int_1^{\infty} z^{\frac{n\beta_2}{\beta_1}} e^{-z} dz$, is the upper incomplete Gamma function [36]. Thus, the SSR coefficient can be obtained in the following form:

$$R = e^2 \sum_{n=0}^{\infty} \frac{(-1)^n}{n!} \boldsymbol{\Gamma}\left(\frac{n\beta_2}{\beta_1} + 1, 1\right). \tag{3.11}$$

Table 2 lists some values of the SSR coefficient obtained from the integral expression in Eq (3.7) and the series expansion (with the upper incomplete gamma function) in Eq (3.11), considering the first 100 terms for some arbitrary parameter values.

Table 2. Some values of the SSR coefficient are obtained from the integral in Eq (3.7) and the series expansion in Eq (3.11).

$\boldsymbol{\alpha}$	$\boldsymbol{\lambda}$	$\boldsymbol{\beta_1}$	$\boldsymbol{\beta_2}$	**Original integral**	**Series expansion**
1.5	0.5	2.0	1.5	0.59620100	0.59620100
0.5	1.5	1.5	1.0	0.63335492	0.63335492
1	0.8	1	0.5	0.71500235	0.71500235
0.2	2.5	3	0.9	0.82010529	0.82389889
1.8	0.7	3.0	1.0	0.80507997	0.80507997
1.8	1.0	1.3	0.2	0.90862185	0.90862185

4. Statistical properties

This section outlines some statistical aspects of the UPGWD, including its QF, moments, and related measures: the mean (μ), variance(σ^2), coefficient of skewness (CS), and coefficient of kurtosis (CK).

4.1. Quantile function and related measures

The QF is an effective tool for generating pseudo-random numbers and conducting Monte Carlo simulations [8]. Additionally, several statistical measures of the UPGWD could potentially be obtained, such as the first quartile, the median (second quartile), and the third quartile, by substituting q with 1/4, 1/2, and 3/4, respectively. In addition to quartiles, other notable quantiles can be calculated, including percentiles, octiles, measures of skewness, and kurtosis. The QF of the UPGWD can be obtained by computing the inverse of its CDF in (2.3) as follows:

$$F^{-1}(q;\boldsymbol{\theta}) = exp\left\{-\left[\frac{[1-ln(q)]^{\frac{1}{\beta}}-1}{\lambda}\right]^{\frac{1}{\alpha}}\right\}, 0 < q < 1. \tag{4.1}$$

Equation (4.1) can be reduced to special cases as follows: $\beta = 1$ and the QF of the UWD of [8]; $\beta = 1,\ \alpha = 2$, and the QF of the unit Rayleigh of [18]; and $\alpha = 1$ and the QF of the unit Nadarajah and Haghighi [19]. It provides a closed-form expression, and this appealing characteristic can be utilized to offer a versatile alternative to the beta quantile regression model, as referenced in [37]. This study primarily aims to present and explore certain aspects of the UPGWD; therefore, the development of quantile regression is not examined in this research and is reserved for future investigations.

4.2. Skewness and kurtosis coefficients

In the context of the QF, two valuable skewness and kurtosis coefficients, which were developed by Bowley [38] and Moors [39], respectively, utilizing the quantiles generated from the QF, are referred to as the Bowley skewness coefficient (BSK) and the Moors kurtosis coefficient (MKU). These metrics are beneficial for several reasons: They serve as alternate coefficients of skewness and kurtosis for distributions where deriving the moments is particularly challenging. Moreover, they exhibit reduced sensitivity to outliers [9]. They can be expressed numerically as

$$BSK = \frac{Q_3+Q_1-2Q_2}{Q_3-Q_1}, \tag{4.2}$$

and

$$MKU = \frac{(O_7-O_5)+(O_3-O_1)}{Q_3-Q_1}, \tag{4.3}$$

where $Q_i = Q(i/4;\boldsymbol{\theta})$ denotes the quartile, while $O_i = Q(i/8;\boldsymbol{\theta})$ represents the octile, both of which can be directly calculated using (4.1).

Figures 2 and 3 show various potential configurations of the BSK and MKU for the UPGWD, corresponding to different parameter values. Furthermore, Table 3 presents values for multiple quantities of the UPGWD, with specific parameter values of α, β, and λ computed according to the QF.

Table 3. Some values of the first quartile, the median, the third quartile, the first octile, the third octile, the fifth octile, the seventh octile, and the MKU and BSK of the UPGWD with selected values of α, λ, and β.

α	λ	β	1st Quar.	Med.	3rd Quar.	1st Oct.	3rd Oct.	5th Oct.	7th Oct.	MKU	BSK
0.5	0.5	0.5	0.0000	0.0006	0.0719	0.0000	0.0000	0.0096	0.3200	4.3164	0.9841
		1.5	0.0432	0.1859	0.4798	0.0115	0.0994	0.3099	0.7057	1.1076	0.3459
	1	0.5	0.0001	0.0239	0.2681	0.0000	0.0029	0.0981	0.5656	1.7550	0.8222
		1.5	0.2077	0.4312	0.6927	0.1072	0.3152	0.5567	0.8400	1.0133	0.0783
	1.5	0.5	0.0019	0.0830	0.4158	0.0000	0.0203	0.2127	0.6840	1.1875	0.6082
		1.5	0.3508	0.5708	0.7829	0.2256	0.4632	0.6767	0.8903	1.0440	-0.0183
1	0.5	0.5	0.0001	0.0239	0.2681	0.0000	0.0029	0.0981	0.5656	1.7550	0.8222
		1.5	0.2077	0.4312	0.6927	0.1072	0.3152	0.5567	0.8400	1.0133	0.0783
	1	0.5	0.0091	0.1546	0.5178	0.0002	0.0537	0.3132	0.7521	0.9680	0.4280
		1.5	0.4558	0.6567	0.8323	0.3274	0.5614	0.7461	0.9165	1.0743	-0.0672
	1.5	0.5	0.0437	0.2881	0.6448	0.0035	0.1424	0.4612	0.8270	0.8397	0.1870
		1.5	0.5923	0.7555	0.8848	0.4750	0.6806	0.8226	0.9436	1.1160	-0.1160
1.5	0.5	0.5	0.0019	0.0830	0.4158	0.0000	0.0203	0.2127	0.6840	1.1875	0.6082
		1.5	0.3508	0.5708	0.7829	0.2256	0.4632	0.6767	0.8903	1.0440	-0.0183
	1	0.5	0.0437	0.2881	0.6448	0.0035	0.1424	0.4612	0.8270	0.8397	0.1870
		1.5	0.5923	0.7555	0.8848	0.4750	0.6806	0.8226	0.9436	1.1160	-0.1160
	1.5	0.5	0.1241	0.4362	0.7464	0.0230	0.2727	0.5969	0.8811	0.8578	-0.0030
		1.5	0.7052	0.8295	0.9216	0.6088	0.7737	0.8780	0.9620	1.1505	-0.1485

Figures 2 and 3 demonstrate that the UPGWD can display negative skewness with a BSK less than zero and positive skewness with BSK greater than 0. At the same time, the MKU indicates that the UPGWD may be classified as platykurtic with MKU < 1.233 and leptokurtic with MKU > 1.233. This conclusion aligns closely with the values presented in Table 3.

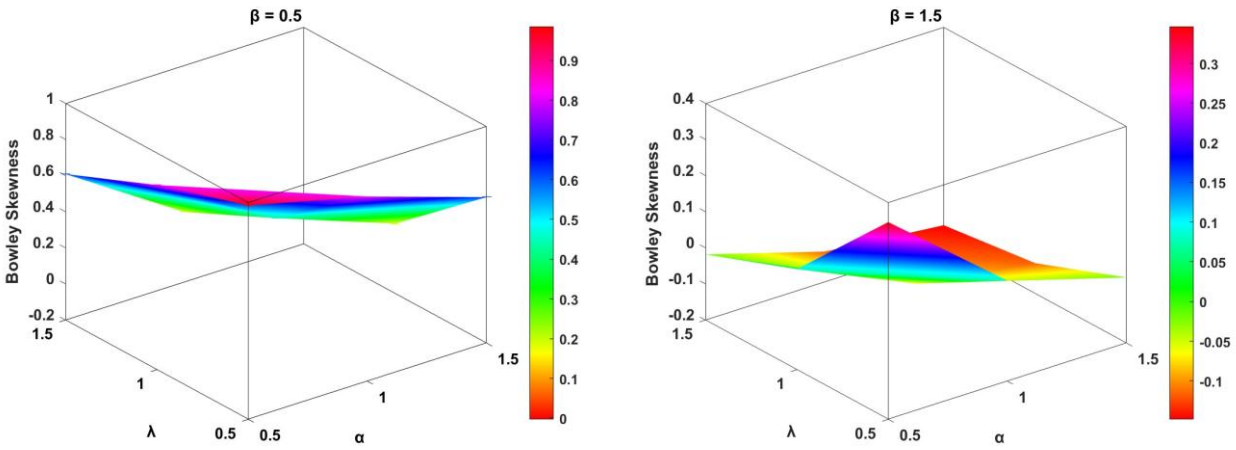

Figure 2. Three-dimensional plots of the Bowley skewness coefficient for the UPGWD.

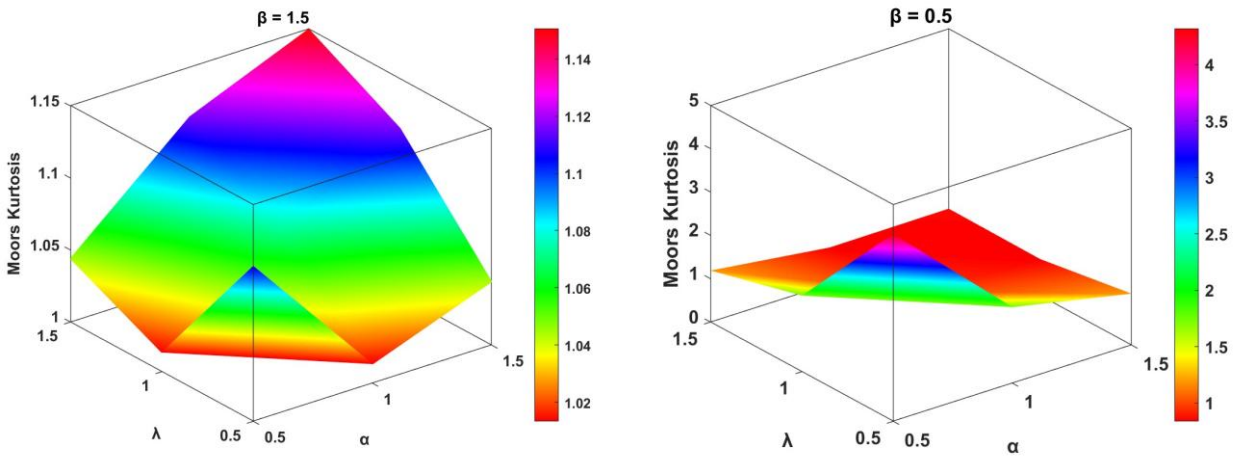

Figure 3. Three-dimensional plots of the Moors kurtosis coefficient for the UPGWD.

4.3. Moments

Finding the moments for every new distribution is crucial for providing meaningful descriptions and explanations of data by supplying basic statistical qualities, such as the central tendency, variability, and the coefficients of skewness and kurtosis. Additionally, it provides a practical approach for estimating parameters for the distribution alongside conventional estimation techniques.

4.3.1. Raw moments

Suppose that V has the UPGWD (α, β, λ). The rth raw moment of V can be found by the following expression:

$$\mu_r' = \mathbb{E}[V^r] = \int_0^1 v^r f(v; \boldsymbol{\theta}) dv$$

$$= \int_0^1 v^r \frac{\alpha\beta\lambda}{v}(-ln\ v)^{\alpha-1}(1+\lambda(-ln\ v)^{\alpha})^{\beta-1} e^{1-(1+\lambda(-ln\ v)^{\alpha})^{\beta}}\, dv. \tag{4.4}$$

After some algebra, we get

$$\mu_r' = 1 - r\int_0^1 v^{r-1}\, e^{1-(1+\lambda(-ln\ v)^{\alpha})^{\beta}} dv = 1 - r\int_0^1 v^{r-1} F(v; \boldsymbol{\theta}) dv. \tag{4.5}$$

This integral can be readily computed numerically using straightforward standard numerical integration procedures and programs in mathematical packages like MATLAB, R, MATHEMATICA, and Python.

Proposition 4.1. *The r*th *raw moments of the UPGWD can also be found in closed form as a series as follows:*

$$\mu_r' = \alpha\beta e \sum_{n,m=0}^{\infty} \frac{(-1)^n}{n!}\left(\frac{\lambda}{r^\alpha}\right)^{m+1} \binom{(n+1)\beta - 1}{m} \boldsymbol{\Gamma}\big(\alpha(m+1)\big).$$

Proof. Considering the exponential function's series expansion in Eq (4.4), we get

$$e^{1-(1+\lambda(-\ln\ v)^\alpha)^\beta} = e.\sum_{n=0}^{\infty} \frac{(-1)^n}{n!}(1+\lambda(-\ln\ v)^\alpha)^{n\beta}.$$

We now plug this expansion back into Eq (4.4)

$$\mu_r' = \alpha\beta\lambda e.\textstyle\sum_{n=0}^{\infty} \frac{(-1)^n}{n!} \int_0^1 v^{r-1}(-\ln\ v)^{\alpha-1}(1+\lambda(-\ln\ v)^\alpha)^{(n+1)\beta-1}\, dv. \tag{4.6}$$

By using Taylor series, we can expand $(1+\lambda(-\ln\ v)^\alpha)^{(n+1)\beta-1}$ *as*

$$(1+\lambda(-\ln\ v)^\alpha)^{(n+1)\beta-1} = \sum_{m=0}^{\infty} \binom{(n+1)\beta - 1}{m} \lambda^m (-\ln\ v)^{\alpha m}.$$

This series converges for all $v \in (0,1)$*, thus, we obtain*

$$\mu_r' = \alpha\beta\ e.\textstyle\sum_{n,m=0}^{\infty} \frac{(-1)^n}{n!} \binom{(n+1)\beta-1}{m} \lambda^{m+1} \int_0^1 v^{r-1}(-\ln\ v)^{\alpha(m+1)-1}\, dv. \tag{4.7}$$

Let $u = -\ln\ v$*; then*

$$\mu_r' = \alpha\beta e.\textstyle\sum_{n,m=0}^{\infty} \frac{(-1)^n}{n!} \binom{(n+1)\beta-1}{m} \lambda^{m+1} \int_0^\infty e^{-ru} u^{\alpha(m+1)-1}\, du. \tag{4.8}$$

where $\int_0^\infty e^{-ru}u^{\alpha(m+1)-1}\, du$ *is the gamma function, and hence*

$$\mu_r' = \alpha\beta e \textstyle\sum_{n,m=0}^{\infty} \frac{(-1)^n}{n!}\left(\frac{\lambda}{r^\alpha}\right)^{m+1} \binom{(n+1)\beta-1}{m} \boldsymbol{\Gamma}\big(\alpha(m+1)\big). \tag{4.9}$$

Given the complexity of this final expression, it is essential to verify the convergence of the expansion series. To confirm that the expression of (4.9) for the *r*th raw moment matches the integral expression (4.5), we computed both numerically for the first six moments. Table 4 demonstrates that the results from both expressions are consistent, exhibiting a difference of approximately zero.

Table 4. The *r*th raw moments of V with the UPGWD (α, β, λ) for some parameter values.

$\boldsymbol{\theta} = (\boldsymbol{\alpha}, \boldsymbol{\beta}, \boldsymbol{\lambda})$			$\boldsymbol{\mu}'_{\boldsymbol{r}}$	**Integration**	**Series expansion**	**Difference**
0.3	1.5	0.1	μ'_1	0.12788	0.12804	0.00016
			μ'_2	0.10490	0.10499	0.00009
			μ'_3	0.09334	0.09340	0.00006
			μ'_4	0.08589	0.08593	0.00005
			μ'_5	0.08050	0.08054	0.00004
			μ'_6	0.07635	0.07638	0.00003
0.5	1	1	μ'_1	0.54564	0.54564	0.00000
			μ'_2	0.43818	0.43818	0.00000
			μ'_3	0.37989	0.37989	0.00000
			μ'_4	0.34135	0.34135	0.00000
			μ'_5	0.31325	0.31325	0.00000
			μ'_6	0.29151	0.29151	0.00000
0.5	1	0.5	μ'_1	0.34135	0.34135	0.00000
			μ'_2	0.25946	0.25946	0.00000
			μ'_3	0.21897	0.21897	0.00000
			μ'_4	0.19347	0.19347	0.00000
			μ'_5	0.17545	0.17545	0.00000
			μ'_6	0.16182	0.16182	0.00000
1.5	0.5	0.1	μ'_1	0.05586	0.07208	0.01622
			μ'_2	0.02189	0.02418	0.00230
			μ'_3	0.01228	0.01299	0.00071
			μ'_4	0.00809	0.00839	0.00031
			μ'_5	0.00583	0.00599	0.00016
			μ'_6	0.00446	0.00455	0.00009
1	1	0.5	μ'_1	0.33333	0.33333	0.00000
			μ'_2	0.20000	0.20000	0.00000
			μ'_3	0.14286	0.14286	0.00000
			μ'_4	0.11111	0.11111	0.00000
			μ'_5	0.09091	0.09091	0.00000
			μ'_6	0.07692	0.07692	0.00000

4.3.2. Central moments

The *r*th central moments of V with the UPGWD (α, β, λ) can be derived directly from Eq (4.5) as follows:

$$\mu_r = \mathbb{E}[(v - \mu)^r] = \sum_{i=0}^{r} \binom{r}{i} (-1)^i \mu^i \, \mu'_{r-i}, \tag{4.10}$$

where $\mu = \mu'_1 = \mathbb{E}[V]$ is the mean (the first raw moment).

Table 5 presents various values of the μ, σ^2, CS, and CK that were numerically calculated for some arbitrarily selected values of α, β, and λ. The CS values in Table 5 reveal the greater flexibility

of the UPGWD in modeling all common types of densities. According to these values, it can be claimed that this distribution can be left-skewed with CS < 0, right-skewed with CS > 0, or almost symmetric with CS approaching zero. On the other hand, the values of the CK exhibit diverse patterns of distribution; these values indicate that the UPGWD is platykurtic with CK < 3 and leptokurtic with CK > 3.

Table 5. Some values of mean, variance, and coefficients of skewness and kurtosis for the UPGWD with selected values of α, β, and λ.

α	β	λ	μ	σ^2	σ	CS	CK
0.3	1.5	0.1	0.1279	0.0885	0.2976	2.1737	6.0747
		0.2	0.2424	0.1422	0.3771	1.1581	2.5794
		0.5	0.5110	0.1770	0.4208	-0.0856	1.2518
		1	0.7679	0.1035	0.3218	-1.3171	3.3035
0.5	1	0.1	0.0838	0.0532	0.2307	2.8976	10.1944
		0.2	0.1589	0.0907	0.3011	1.7855	4.6790
		0.5	0.3414	0.1429	0.3781	0.6073	1.7205
		1	0.5456	0.1405	0.3748	-0.2371	1.4724
1	1	0.1	0.0909	0.0394	0.1984	2.6609	9.5665
		0.2	0.1667	0.0631	0.2513	1.6583	4.7143
		0.5	0.3333	0.0889	0.2981	0.6389	2.1429
		1	0.5000	0.0833	0.2887	0.0000	1.8000
1.5	0.5	0.1	0.0559	0.0188	0.1370	3.4867	16.2522
		0.2	0.0988	0.0315	0.1775	2.3968	8.6155
		0.5	0.1910	0.0531	0.2305	1.3590	3.9946
		1	0.2894	0.0672	0.2592	0.7609	2.5174

4.3.3. Moment-generating function

The moment-generating function (MGF) of a random variable V with the UPGWD (α, β, λ) is defined as

$$M_V(t) = \mathbb{E}[e^{tV}] = \int_0^1 e^{tv} f(v; \boldsymbol{\theta}) dv = \sum_{r=0}^{\infty} \frac{t^r}{r!} \mu'_r. \tag{4.11}$$

By substituting the moments in Eq (4.5), we get

$$M_V(t) = \sum_{r=0}^{\infty} \frac{t^r}{r!} \left[1 - r \int_0^1 v^{r-1} F(v; \boldsymbol{\theta}) dv\right]. \tag{4.12}$$

After some algebra, we obtained

$$M_V(t) = e^t - t \int_0^1 e^{tv} F(v; \boldsymbol{\theta}) dv. \tag{4.13}$$

An alternative expression for the MGF can be obtained via Eq (4.9) as follows:

$$M_V(t) = \alpha\beta e \sum_{n,m,r=0}^{\infty} \frac{(-1)^n t^r}{n!r!} \left(\frac{\lambda}{(r+1)^{\alpha}}\right)^{m+1} \binom{(n+1)\beta-1}{m} \boldsymbol{\Gamma}\left(\alpha(m+1)\right). \tag{4.14}$$

The MGF is a crucial notion in probability theory that facilitates the derivation of key statistical characteristics, such as the central tendency and variability measures of a random variable [26].

4.3.4. Incomplete moments

It is of some interest to find the incomplete moments of V with the UPGWD (α, β, λ). Incomplete moments serve as a crucial conceptual structure in economics, especially in the analysis of income distribution. Their use makes it easier to calculate essential metrics like the mean deviations, inequality indices like the Pietra and Gini coefficients, and Lorenz and Bonferroni curves. The rth incomplete moment is derived by modifying the raw moment formula by introducing an upper limit $0 < t \leq 1$ as follows:

$$I_r(t) = \mathbb{E}[V^r | 0 < t \leq 1] = \int_0^t v^r f(v; \boldsymbol{\theta}) dv$$

$$= \int_0^t v^r \frac{\alpha\beta\lambda}{v} (-ln\ v)^{\alpha-1} (1 + \lambda(-ln\ v)^{\alpha})^{\beta-1} e^{1-(1+\lambda(-ln\ v)^{\alpha})^{\beta}}\, dv. \tag{4.15}$$

After some algebra, we obtain the rth incomplete moment as follows:

$$I_r(t) = t^r e^{1-(1+\lambda(-ln\ t)^{\alpha})^{\beta}} - r \int_0^t v^{r-1} e^{1-(1+\lambda(-ln\ v)^{\alpha})^{\beta}} dv$$

$$= t^r F(t; \boldsymbol{\theta}) - r \int_0^t v^{r-1} F(v; \boldsymbol{\theta}) dv. \tag{4.16}$$

Alternatively, the rth incomplete moment can be obtained via Eq (4.9) as

$$I_r(t) = \alpha\beta e \sum_{n,m=0}^{\infty} \frac{(-1)^n}{n!} \left(\frac{\lambda}{r^{\alpha}}\right)^{m+1} \binom{(n+1)\beta-1}{m} \gamma\left(\alpha(m+1), -rln(t)\right), \tag{4.17}$$

where $\gamma\left(\alpha(m+1), -rln(t)\right)$ is the lower incomplete gamma function.

5. Additional properties

This section delineates some additional statistical aspects of the UPGWD, including the mean deviation, inequality measures, and order statistics.

5.1. Mean deviation

The mean deviation (MD) about μ is known as the average of the absolute deviations of each data point from its mean. The MD can be mathematically represented as

$$MD = \mathbb{E}(|v-\mu|) = 2\mu F(U;\boldsymbol{\theta}) - 2\int_0^{\mu} v\, f(v;\boldsymbol{\theta})dv = 2\mu F(\mu;\boldsymbol{\theta}) - 2I_1(\mu), \tag{5.1}$$

where $\mu_1'(\mu)$ is the first incomplete moment

$$I_1(\mu) = \alpha\beta e \sum_{n,m=0}^{\infty} \frac{(-1)^n}{n!}\lambda^{m+1}\binom{(n+1)\beta-1}{m}\gamma\left(\alpha(m+1), -ln(\mu)\right).$$

Hence

$$MD = 2\mu F(\mu;\theta) - 2\alpha\beta e \sum_{n,m=0}^{\infty} \frac{(-1)^n}{n!}\lambda^{m+1}\binom{(n+1)\beta-1}{m}\gamma\left(\alpha(m+1), -ln(\mu)\right). \tag{5.2}$$

5.2. Inequality measures

One of the most critical empirical applications of the incomplete moments is that it can enhance empirical elucidations of the distributions and inequality measures, including the commonly utilized Lorenz and Bonferroni curves for evaluating income and wealth disparity. The Lorenz curve (LC) and Bonferroni curve (BC) are economic and statistical graphs that show a population's income or wealth disparity. Although the LC and BC are similar, they highlight distinct features of income distribution. The LC shows income inequality by indicating the cumulative distribution of income or wealth. Building on the LC, the BC adds inequality indicators to analyze income distribution more deeply. They help economists and scholars understand resource allocation and economic inequality. Both curves reveal economic disparity, although the LC is more popular, while the BC focuses on the lower end. Whether the LC prioritizes inequality or the BC concentrates on poverty determines the selection. The LC and BC can be computed as

$$LC(p) = \frac{I_1(p)}{\mu} = \frac{1}{\mu}\int_0^{p} vf(v;\boldsymbol{\theta})dv, \tag{5.3}$$

$$BC(p) = \frac{LC(p)}{F(p)} = \frac{I_1(p)}{F(p)\mu}, \tag{5.4}$$

where $I_1(p)$ is the first incomplete moment, p is the QF given by (4.1), and $F(p)$ is a proportion of units with income less than or equal to p. For the UPGWD, the LC and BC can be given by

$$LC(p) = \frac{\alpha\beta e}{\mu} \sum_{n,m=0}^{\infty} \frac{(-1)^n}{n!}\lambda^{m+1}\binom{(n+1)\beta-1}{m}\gamma\left(\alpha(m+1), -ln(p)\right). \tag{5.5}$$

$$BC(p) = \frac{\alpha\beta e}{F(p)\mu} \sum_{n,m=0}^{\infty} \frac{(-1)^n}{n!}\lambda^{m+1}\binom{(n+1)\beta-1}{m}\gamma\left(\alpha(m+1), -ln(p)\right). \tag{5.6}$$

5.3. Order statistics

Order statistics are an essential concept in statistical analysis, facilitating the investigation of extreme values and the inherent properties of random variables. They are vital for enabling conclusions regarding the population from which the sample is derived. The values in a sample, arranged in ascending order, provide insights into the data's distribution and sample characteristics. Their

components encompass minimum and maximum values, as well as percentiles like the median and quartiles, which exemplify the data's distribution and central tendency. The sth-order statistics of a random sample with size n from the UPGWD have the following PDF:

$$f_{V_{(s)}}(v) = \frac{n!}{(s-1)!(n-s)!}[F_V(v)]^{s-1}[1-F_V(v)]^{n-s}f_V(v), \tag{5.7}$$

where $F_V(v)$ is the CDF of the UPGWD (2.3) and $f_V(v)$ is the PDF (2.4); thus, we obtain

$$f_{V_{(s)}}(v) = \frac{n!}{(s-1)!\,(n-s)!}\left[e^{1-(1+\lambda(-ln\ v)^{\alpha})^{\beta}}\right]^{s-1}\left[1-e^{1-(1+\lambda(-ln\ v)^{\alpha})^{\beta}}\right]^{n-s}$$

$$\times\frac{\alpha\beta\lambda}{v}(-ln\ v)^{\alpha-1}(1+\lambda(-ln\ v)^{\alpha})^{\beta-1}e^{1-(1+\lambda(-ln\ v)^{\alpha})^{\beta}}. \tag{5.8}$$

After some algebra, we obtain

$$f_{V_{(s)}}(v) = \frac{n!\alpha\beta\lambda(-ln\ v)^{\alpha-1}(1+\lambda(-ln\ v)^{\alpha})^{\beta-1}}{v(s-1)!(n-s)!}\sum_{i=0}^{\infty}\binom{n-s}{i}(-1)^i\,e^{(s+i)\left(1-(1+\lambda(-ln\ v)^{\alpha})^{\beta}\right)}. \tag{5.9}$$

6. Estimation

This section addresses estimating the parameters of the UPGWD using the MLE technique. It is a prevalent statistical method for estimating the unknown parameters of a distribution. It operates on the principle of selecting the parameter value that maximizes the probability of the observed data. For a random sample $V = (v_1, v_2, \dots, v_n)$ of size n from the UPGWD with the parameter vector $\boldsymbol{\theta} = (\alpha, \beta, \lambda)^T$, the likelihood function can be articulated as

$$L(\boldsymbol{\theta}) = \prod_{i=1}^{n} f(v_i;\boldsymbol{\theta})$$

$$= (\alpha\beta\lambda)^n e^{n-\sum_{i=1}^{n}[1+\lambda(-ln\ v_i)^{\alpha}]^{\beta}}\prod_{i=1}^{n}\frac{1}{v_i}(-ln\ v_i)^{\alpha-1}(1+\lambda(-ln\ v_i)^{\alpha})^{\beta-1}. \tag{6.1}$$

By taking the natural logarithm for $L(\boldsymbol{\theta})$, the log-likelihood function $\ell(\boldsymbol{\theta})$ can be obtained as follows:

$$\ell(\boldsymbol{\theta}) = n(ln\alpha + ln\beta + ln\lambda) + n - \sum_{i=1}^{n}(1+\lambda(-ln\ v_i)^{\alpha})^{\beta} - \sum_{i=1}^{n} ln\ v_i + (\alpha-1)\sum_{i=1}^{n} ln(-ln\ v_i)$$

$$+(\beta-1)\sum_{i=1}^{n} ln(1+\lambda(-ln\ v_i)^{\alpha}). \tag{6.2}$$

Then, by finding the first partial derivative for (6.2) concerning α, β, and λ, we get the score functions as follows:

$$\frac{\partial \ell(\boldsymbol{\theta})}{\partial \alpha} = \frac{n}{\alpha} - \lambda b \sum_{i=1}^{n} (-ln\ v_i)^{\alpha} ln(-ln\ v_i)(1 + \lambda(-ln\ v_i)^{\alpha})^{\beta-1} + \sum_{i=1}^{n} ln(-ln\ v_i)$$

$$+(\beta - 1)\lambda \sum_{i=1}^{n} \frac{(-ln\ v_i)^{\alpha} ln(-ln\ v_i)}{[1+\lambda(-ln\ v_i)^{\alpha}]}, \tag{6.3}$$

$$\frac{\partial \ell(\boldsymbol{\theta})}{\partial \beta} = \frac{n}{\beta} - \sum_{i=1}^{n} (1 + \lambda(-ln\ v_i)^{\alpha})^{\beta} ln(1 + \lambda(-ln\ v_i)^{\alpha}) + \sum_{i=1}^{n} ln[1 + \lambda(-ln\ v_i)^{\alpha}], \tag{6.4}$$

$$\frac{\partial \ell(\boldsymbol{\theta})}{\partial \lambda} = \frac{n}{\lambda} - \beta \sum_{i=1}^{n} (-ln\ v_i)^{\alpha} (1 + \lambda(-ln\ v_i)^{\alpha})^{\beta-1} + (\beta - 1) \sum_{i=1}^{n} \frac{(-ln\ v_i)^{\alpha}}{[1+\lambda(-ln\ v_i)^{\alpha}]}. \tag{6.5}$$

Finally, by setting Eqs (6.3)–(6.5) equal to zero and solving them with the help of an iterative aspect algorithm (e.g., the gradient ascent, Newton–Raphson, or quasi-Newton methods) to estimate the parameters $\boldsymbol{\theta} = (\alpha, \beta, \lambda)$.

6.1. Existence of the MLE

The MLE exists if $\ell(\boldsymbol{\theta})$ reaches a global maximum in the parameter space $\Theta = (\alpha, \beta, \lambda) \in \mathbb{R}^+ \times \mathbb{R}^+ \times \mathbb{R}^+$ [40]. By restricting Θ to a compact subset (for example, $\alpha, \beta, \lambda \in [\varepsilon, M]$ where $\varepsilon > 0$ and $M < \infty$), $\ell(\boldsymbol{\theta})$ is continuous in $\boldsymbol{\theta}$, and the extreme value theorem guarantees the existence of a maximum within this compact set. Moreover, we analyze the behavior of $\ell(\boldsymbol{\theta})$ as any parameter approaches the boundary of Θ. For instance, as $\alpha \to 0^+$, the term $(-lnv_i)^{\alpha} \to 1$, but the component $(\alpha - 1)ln(-ln\ v_i)$ dominates and $\ell(\boldsymbol{\theta}) \to -\infty$. Similar behavior is observed as any parameter tends to $0^+ or\ \infty$, ensuring the maximum is reached in the interior; i.e., $\ell(\boldsymbol{\theta})$ is continuous in $\boldsymbol{\theta} = (\alpha, \beta, \lambda)$ over the compact set $\Theta = [\varepsilon, M]^3$ for a sufficiently small $\varepsilon > 0$ and a large M. As $\alpha, \beta,$ or λ approach the boundary of Θ, $\ell(\boldsymbol{\theta}) \to -\infty$. Thus, by the extreme value theorem, the MLE exists and lies in the interior of Θ.

6.2. Regularity conditions

According to [40,41], the MLE is consistent, asymptotically normal, and efficient if $\ell(\boldsymbol{\theta})$ is at least twice differentiable concerning $\boldsymbol{\theta}$. The model is identifiable, meaning that $\boldsymbol{\theta} \neq \boldsymbol{\theta}' \Rightarrow f(v_i; \boldsymbol{\theta}) \neq f(v_i; \boldsymbol{\theta}')$; i.e., different parameter values yield distinct distributions. The Fisher information matrix (FIM) $I_{(n)}(\boldsymbol{\theta})$, defined as the negative expected Hessian, is positive definite. The true parameter vector $\boldsymbol{\theta}^0$ must lie in the interior of Θ.

6.3. Asymptotic confidence intervals

The FIM $I_{(n)}(\boldsymbol{\theta})$ is used for estimating the intervals of α, β, and λ to derive the standard errors of point estimates, formulate confidence intervals, and conduct hypothesis testing. The matrix elements may be derived as follows:

$$I_{(n)}(\boldsymbol{\theta}) = -\mathbb{E}\begin{pmatrix} \frac{\partial^2 \ell(\boldsymbol{\theta})}{\partial \alpha^2} & \frac{\partial^2 \ell(\boldsymbol{\theta})}{\partial \alpha \partial \beta} & \frac{\partial^2 \ell(\boldsymbol{\theta})}{\partial \alpha \partial \lambda} \\ \frac{\partial^2 \ell(\boldsymbol{\theta})}{\partial \alpha \partial \beta} & \frac{\partial^2 \ell(\boldsymbol{\theta})}{\partial \beta^2} & \frac{\partial^2 \ell(\boldsymbol{\theta})}{\partial \beta \partial \lambda} \\ \frac{\partial^2 \ell(\boldsymbol{\theta})}{\partial \alpha \partial \lambda} & \frac{\partial^2 \ell(\boldsymbol{\theta})}{\partial \beta \partial \lambda} & \frac{\partial^2 \ell(\boldsymbol{\theta})}{\partial \lambda^2} \end{pmatrix}.$$

By setting $u_i = -\ln\ v_i, i = 1, \ldots, \ldots, n$, the elements of the FIM can be obtained as follows:

$$\frac{\partial^2 \ell(\boldsymbol{\theta})}{\partial \alpha^2} = -\frac{n}{\alpha^2} + (\beta - 1)\sum_{i=1}^{n} \frac{\left[\lambda u_i^{\alpha} (lnu_i)^2 \left(1 + \lambda u_i^{\alpha}(1 - \alpha lnu_i)\right)\right]}{(1 + \lambda u_i^{\alpha})^2}$$

$$-\beta \sum_{i=1}^{n} \lambda\, u_i^{\alpha} (lnu_i)^2 (1 + \lambda u_i^{\alpha})^{\beta-2}\left(1 + \lambda u_i^{\alpha}(1 + \beta\lambda u_i^{\alpha})\right), \tag{6.6}$$

$$\frac{\partial^2 \ell(\boldsymbol{\theta})}{\partial \beta^2} = -\frac{n}{\beta^2} - \sum_{i=1}^{n} (1 + \lambda u_i^{\alpha})^{\beta} [ln(1 + \lambda u_i^{\alpha})]^2, \tag{6.7}$$

$$\frac{\partial^2 \ell(\boldsymbol{\theta})}{\partial \lambda^2} = \frac{-n}{\lambda^2} - (\beta - 1)\sum_{i=1}^{n} \left[\frac{u_i^{2\alpha}}{(1+\lambda u_i^{\alpha})^2}\right] - \beta(\beta - 1)\sum_{i=1}^{n} u_i^{2\alpha} (1 + \lambda u_i^{\alpha})^{\beta-2}, \tag{6.8}$$

$$\frac{\partial^2 \ell(\boldsymbol{\theta})}{\partial \alpha \partial \beta} = \sum_{i=1}^{n} \left[\frac{\lambda u_i^{\alpha} lnu_i}{(1+\lambda u_i^{\alpha})}\right] - \sum_{i=1}^{n} \lambda\, u_i^{\alpha} lnu_i (1 + \lambda u_i^{\alpha})^{\beta-1}[1 + \beta ln(1 + \lambda u_i^{\alpha})], \tag{6.9}$$

$$\frac{\partial^2 \ell(\boldsymbol{\theta})}{\partial \alpha \partial \lambda} = \frac{(\beta-1)}{\lambda}\sum_{i=1}^{n} \left[\frac{u_i^{\alpha} lnu_i}{(1+\lambda u_i^{\alpha})}\right] - \beta \sum_{i=1}^{n} u_i^{\alpha} ln\, u_i (1 + \lambda u_i^{\alpha})^{\beta-1}[1 + \beta\lambda u_i^{\alpha}], \tag{6.10}$$

$$\frac{\partial^2 \ell(\boldsymbol{\theta})}{\partial \beta \partial \lambda} = \frac{1}{\lambda}\sum_{i=1}^{n} \left[\frac{u_i^{\alpha}}{(1+\lambda u_i^{\alpha})}\right] - \sum_{i=1}^{n} u_i^{\alpha} (1 + \lambda u_i^{\alpha})^{\beta-1}[1 + \beta ln(1 + \lambda u_i^{\alpha})]. \tag{6.11}$$

The asymptotic distribution of $\widehat{\boldsymbol{\theta}}$ goes to $N(0, I^{-1})$, and the asymptotic $(1-\delta)\,100\%$ confidence interval for $\boldsymbol{\theta} = (\alpha, \beta, \lambda)^T$ can be resolved as

$$ACI_{(1-\delta)}(\alpha) = \hat{\alpha} \pm z_{\delta/2}\sqrt{Var\hat{\alpha}},$$

$$ACI_{(1-\delta)}(\beta) = \hat{\beta} \pm z_{\delta/2}\sqrt{Var\hat{\beta}},$$

$$ACI_{(1-\delta)}(\lambda) = \hat{\lambda} \pm z_{\delta/2}\sqrt{Var\hat{\lambda}},$$

where $Var\hat{\alpha}$, $Var\hat{\beta}$, and $Var\hat{\lambda}$ are the asymptotic variances obtained from the diagonal elements of $I^{-1}(\boldsymbol{\theta})$, the inverse of the Fisher matrix, and $z_{\delta/2}$ is the upper qth quantile from the standard normal distribution, respectively. The elements of the matrix are numerically computed using the maximization functions available in mathematical packages like MATLAB, R, MATHEMATICA, and Python. As discussed above, we addressed the existence and regularity conditions for the MLE in our model.

- Existence: $\ell(\boldsymbol{\theta})$ is continuous and coercive (i.e., $\ell(\boldsymbol{\theta}) \to -\infty$ as $\| \boldsymbol{\theta} \| \to \infty$ or $\boldsymbol{\theta}$ approaches the boundary of Θ), ensuring that a finite maximum exists in the interior of Θ.
- Regularity: The UPGWD satisfies the following standard regularity conditions:
  - The support of v_i does not depend on $\boldsymbol{\theta}$;
  - $\ell(\boldsymbol{\theta})$ is twice differentiable in $\boldsymbol{\theta}$;
  - The FIM is positive definite at $\boldsymbol{\theta}^0$ (verified numerically for simulated data in Section 7).

7. Simulation

This section is dedicated to conducting a simulation study using the Monte Carlo simulation (MCS) algorithm to assess the efficacy of the MLE approach previously mentioned for estimating the parameters of the UPGWD. MCS is a robust method used to produce random simulated data that closely resemble real-world conditions. This simulation enables us to gain a deeper understanding of the MLE technique's behavior and examine its characteristics. The assessment of the point estimation of α, β, and λ is performed using the mean squared errors (MSE) and bias. Furthermore, to assess the interval estimate, we use the 95% coverage probability (CP95%) with δ = 5% for each parameter. The simulation procedures are conducted following Algorithm 1.

Algorithm 1: Monte Carlo simulation.

1. ***Inputs***
2. True parameters (α, β, λ):
3. Set 1: = (1.8, 0.4, 0.7),
4. Set 2: = (0.5, 0.5, 0.5),
5. Set 3: = (1.5, 0.5, 0.5),
6. Set 4: = (1.4, 0.6, 0.4),
7. Set 5: = (1.4, 0.6, 1.0).
8. Sample sizes: $n \in$ {75, 100, 120, 150, 250, 300}
9. Number of simulations = 1000.
10. ***Step 1:*** Generate random samples with different sizes *n* using the inverse CDF of the UPGWD in Eq (4.1).
11. ***Step 2:*** Estimate the parameter vector $\boldsymbol{\theta} = (\alpha, \beta, \lambda)^T$ using the MLE for each sample size and repeat this process 1000 times using the Fminsearch optimization function.
12. ***Step 3:*** Compute the mean, bias, and MSE for each sample size as follows:

$$Mean = \frac{1}{1000}\sum_{i=1}^{1000} \widehat{\boldsymbol{\theta}}_i, \qquad Bias = \frac{1}{1000}\sum_{i=1}^{1000} \left(\widehat{\boldsymbol{\theta}}_i - \boldsymbol{\theta}\right), \qquad and\ MSE = \frac{1}{1000}\sum_{i=1}^{1000} \left(\widehat{\boldsymbol{\theta}}_i - \boldsymbol{\theta}\right)^2.$$

13. ***Step 4:*** Compute the coverage probabilities ($CP_{95\%}$) of $\alpha, \beta,$ and λ for each sample size.

$$CI_{(95\%)} = \widehat{\boldsymbol{\theta}} \pm 1.96\frac{\sigma\left(\widehat{\boldsymbol{\theta}}\right)}{\sqrt{n}}, CP95\% = \frac{1}{1000}\sum_{i=1}^{R} \mathbb{I}\left[\boldsymbol{\theta}_{true} \in [LCI_i, UCI_i]\right].$$

14. ***Step 5: Output***
15. Tables of MSE, bias, mean estimates, and $CP_{95\%}$ for each *n* and each parameter set.

The simulation results provided in Tables 6–10 illustrate the precision of the MLE in estimating the parameters of the UPGWD. It is visible from these tables that the following further observations can be made:

- The estimated values of the parameters approach their actual values, indicating the improved accuracy and consistency of the estimator.
- The larger the sample size, the smaller the bias and MSE; moreover, as the sample size increases, their values tend to zero.
- The CP95% often converges to the nominal 95% level as the sample size increases.

The results indicate that the MLE operates consistently for moderate to large sample sizes. However, some inconsistencies related to the CP95% are noted. These discrepancies may be attributed to the use of asymptotic normal approximations in small samples. Therefore, we will consider alternative inference methods in future research, such as bootstrap confidence intervals, to improve the accuracy of coverage.

Moreover, Figures 4–8 assess the behavior of the estimator across various sample sizes. In summary, the simulation study confirms the robustness of the MLE for the UPGWD as the sample sizes increase. On the basis of these results, we consider the MLE for estimating UPGWD parameters in real-world application analysis in the following section.

Table 6. MCS results (Case I).

θ	n	Mean	Bias	MSE	$CP_{95\%}$
$\alpha = 1.8$	75	1.9394	0.1394	0.2808	0.835
	100	1.8745	0.0745	0.1790	0.890
	120	1.8551	0.0551	0.1310	0.918
	150	1.8451	0.0451	0.1067	0.940
	250	1.8149	0.0149	0.0517	0.949
	300	1.8047	0.0047	0.0447	0.950
$\beta = 0.4$	75	0.5153	0.1153	0.9565	0.788
	100	0.4452	0.0527	0.1540	0.795
	120	0.4527	0.0452	0.0417	0.872
	150	0.4281	0.0281	0.0183	0.882
	250	0.4201	0.0201	0.0097	0.951
	300	0.4081	0.0081	0.0063	0.958
$\lambda = 0.7$	75	0.8518	0.1518	0.5409	0.726
	100	0.7798	0.0798	0.3019	0.758
	120	0.7490	0.0490	0.1535	0.810
	150	0.7409	0.0409	0.1199	0.827
	250	0.7234	0.0234	0.0524	0.901
	300	0.7192	0.0192	0.0475	0.929

Table 7. MCS results (Case II).

θ	n	Mean	Bias	MSE	$CP_{95\%}$
$\alpha = 0.5$	75	0.4992	-0.0008	0.0001	0.999
	100	0.49996	-3.98E-05	2.93E-05	0.998
	120	0.5000	0.0000	0.0000	1
	150	0.5000	0.0000	0.0000	1
	250	0.5000	0.0000	0.0000	1
	300	0.5000	0.0000	0.0000	1
$\beta = 0.5$	75	0.5620	0.0620	1.2771	0.967
	100	0.5017	0.0017	0.0014	0.997
	120	0.5000	0.0000	0.0000	1
	150	0.5000	0.0000	0.0000	1
	250	0.5000	0.0000	0.0000	1
	300	0.5000	0.0000	0.0000	1
$\lambda = 0.5$	75	0.4964	-0.0036	0.0014	0.994
	100	0.4992	-0.0008	0.0002	0.997
	120	0.5000	0.0000	0.0000	1
	150	0.5000	0.0000	0.0000	1
	250	0.5000	0.0000	0.0000	1
	300	0.5000	0.0000	0.0000	1

Table 8. MCS results (Case III).

θ	n	Mean	Bias	MSE	$CP_{95\%}$
$\alpha = 1.5$	75	1.5530	0.0530	0.1381	0.915
	100	1.5512	0.0512	0.1205	0.930
	120	1.5465	0.0465	0.0840	0.918
	150	1.5386	0.0386	0.0677	0.940
	250	1.5149	0.0149	0.0352	0.949
	300	1.5002	0.0002	0.0289	0.956
$\beta = 0.5$	75	0.7259	0.2259	3.5610	0.856
	100	0.6335	0.1335	2.1000	0.931
	120	0.5772	0.0772	0.2579	0.907
	150	0.5501	0.0501	0.0599	0.924
	250	0.5284	0.0284	0.0182	0.949
	300	0.5162	0.0162	0.0125	0.955
$\lambda = 0.5$	75	0.5442	0.0442	0.1422	0.874
	100	0.5357	0.0357	0.0758	0.854
	120	0.5324	0.0324	0.0709	0.867
	150	0.5249	0.0249	0.0491	0.895
	250	0.5080	0.0080	0.0239	0.895
	300	0.5027	0.0027	0.0179	0.940

Table 9. MCS results (Case IV).

θ	n	Mean	Bias	MSE	$CP_{95\%}$
$\alpha = 1.4$	75	1.4890	0.0890	0.1884	0.901
	100	1.4427	0.0427	0.0886	0.908
	120	1.4381	0.0381	0.0618	0.916
	150	1.4155	0.0155	0.0512	0.924
	250	1.4082	0.0082	0.0276	0.933
	300	1.4018	0.0018	0.0232	0.948
$\beta = 0.6$	75	0.9335	0.3335	4.2806	0.848
	100	0.8714	0.2714	2.4472	0.865
	120	0.7214	0.1214	0.5890	0.906
	150	0.6860	0.0860	0.0907	0.918
	250	0.6470	0.0470	0.0364	0.925
	300	0.6324	0.0324	0.0270	0.948
$\lambda = 0.4$	75	0.4513	0.0513	0.2210	0.767
	100	0.4213	0.0213	0.0644	0.808
	120	0.4193	0.0193	0.0424	0.829
	150	0.4079	0.0079	0.0304	0.912
	250	0.4024	0.0024	0.0168	0.931
	300	0.4022	0.0022	0.0127	0.943

Table 10. MCS results (Case V).

θ	n	Mean	Bias	MSE	$CP_{95\%}$
$\alpha = 1.4$	75	1.4662	0.0662	0.1209	0.821
	100	1.4593	0.0593	0.0921	0.882
	120	1.4413	0.0413	0.0655	0.885
	150	1.4391	0.0391	0.0516	0.862
	250	1.4226	0.0226	0.0284	0.937
	300	1.4199	0.0199	0.0260	0.952
$\beta = 0.6$	75	1.0437	0.4437	5.7884	0.858
	100	0.7273	0.1273	0.7877	0.888
	120	0.7233	0.1233	0.5277	0.851
	150	0.6765	0.0765	0.1143	0.902
	250	0.6324	0.0324	0.0322	0.894
	300	0.6322	0.0322	0.0333	0.927
$\lambda = 1$	75	1.3937	0.3937	2.0740	0.810
	100	1.3070	0.3070	1.2272	0.899
	120	1.1495	0.1495	0.6309	0.918
	150	1.1052	0.1052	0.4389	0.910
	250	1.0638	0.0638	0.1838	0.907
	300	1.0545	0.0545	0.1712	0.920

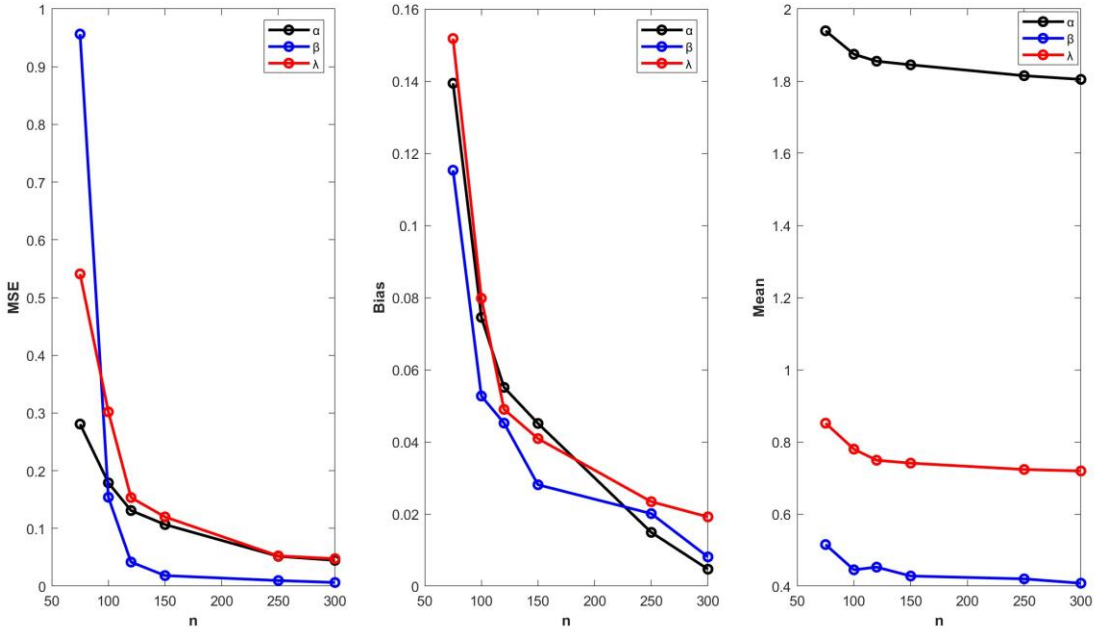

Figure 4. Graphical depiction of the simulation results for $\alpha = 1.8$, $\beta = 0.4$, and $\lambda = 0.7$.

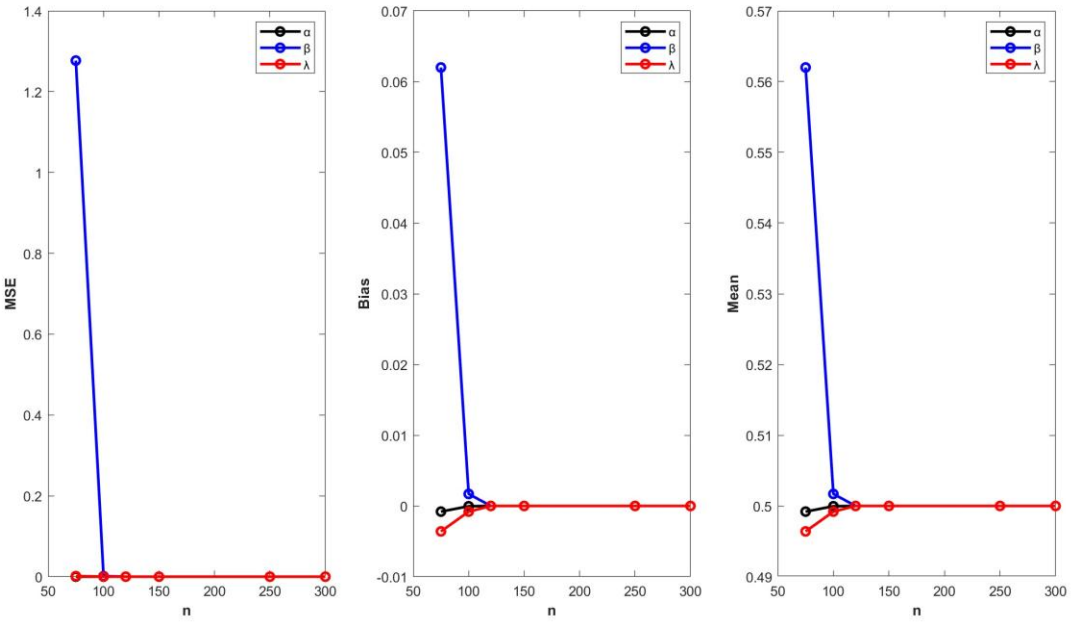

Figure 5. Graphical depiction of the simulation results for $\alpha = 0.5$, $\beta = 0.5$, and $\lambda = 0.5$.

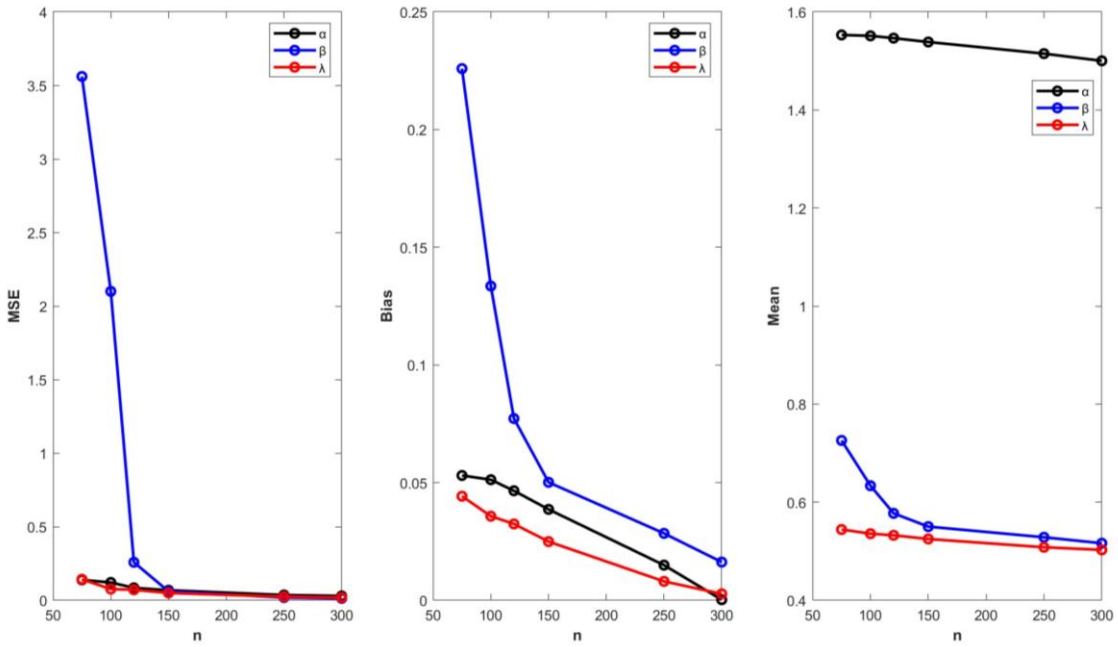

Figure 6. Graphical depiction of the simulation results for $\alpha = 1.5$, $\beta = 0.5$, and $\lambda = 0.5$.

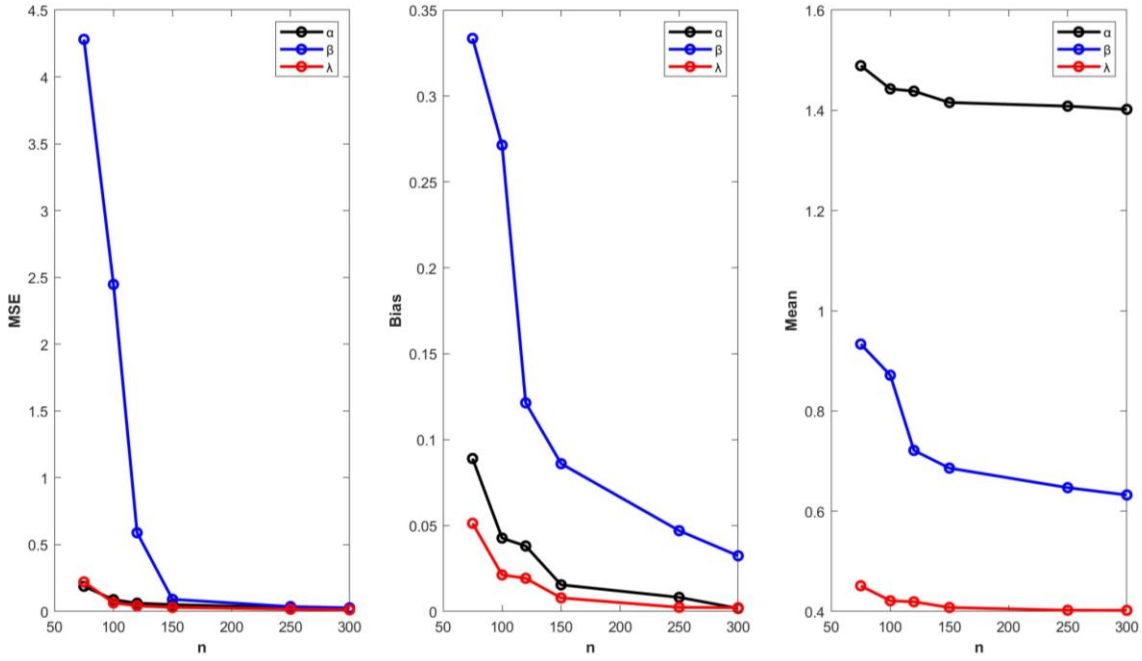

Figure 7. Graphical depiction of the simulation results for $\alpha = 1.4$, $\beta = 0.6$, and $\lambda = 0.4$.

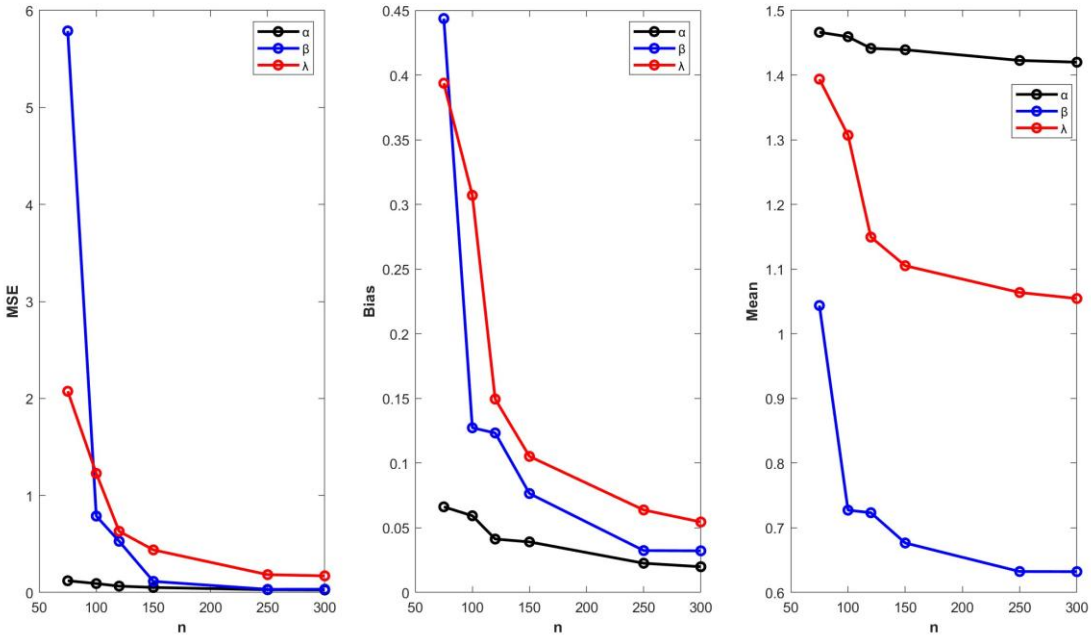

Figure 8. Graphical depiction of the simulation results for $\alpha = 1.4$, $\beta = 0.6$, and $\lambda = 1$.

8. Real-world data analysis

This section's primary aim is to demonstrate the potential importance of the UPGWD, highlighting its flexibility and ability to model real lifetime data from diverse domains with varying types and sizes of data.

- Given the fact that the UPGWD has three parameters, it offers more control over all common types of data, whether left-skewed data, positively skewed data, platykurtic, leptokurtic, or mesokurtic data, as shown in Figure 1.
- Additionally, its HRF, with a bathtub-shaped pattern, shows that it can be beneficial and valuable for modeling data related to the medical sector, reliability engineering, and other practical domains.
- According to [42], the HRF of the medical data often demonstrates a bathtub shape. In such a case, our proposed model may be the optimal choice due to its greater flexibility in modeling all common types of hazard rates, including the bathtub shape.

To that end, we present four real-world datasets related to COVID-19 mortality rates, reliability, engineering, and radiation (all datasets are provided in the Appendix).

- **The first dataset** related to the COVID-19 pandemic represents 61 days of COVID-19 mortality rates in the Kingdom of Saudi Arabia from 6 July 2021 to 4 September 2021; it was first provided by [43] and reintroduced in [9].

- **The second dataset** initially studied by [44], consists of the failure times (FT) of an airplane's air-cooling system (in hours). We execute a normalization procedure by dividing each value by 265, resulting in a transformed dataset ranging from 0 to 1.

- **The third dataset** concerns the burr measurements (BMs) on iron sheets. It consists of 50 observations on burr (in millimeters), with a hole diameter of 9 mm and a sheet thickness of 2 mm. This dataset was initially presented by [45].

- **The fourth dataset** pertains to the susceptibility index (SI) for both irradiated and unirradiated peppermint packages. This dataset, originally given by [46], examines the vulnerability of both irradiated and unirradiated peppermint sachets to infestation by the pharmacy beetle. We applied the transformation e^{-x_i} to each value, resulting in a transformed dataset ranging from 0 to 1.

Some descriptive statistics for these datasets are presented in Table 11, which reveals that the COVID-19 dataset is left-skewed and platykurtic due to its negative CS and CK < 3. Contrary to the first dataset, the second dataset is right-skewed and leptokurtic with CK > 3. Table 11 also exhibits that the third dataset has a CS approaching zero and CK < 3, which means that this dataset is relatively symmetric and platykurtic. The fourth dataset is positively skewed and platykurtic.

Table 11. Some descriptive statistics for the datasets.

Datasets	*N*	Mean	Std_dev.	1st Q.	Median	3rd Q.	CS	CK
COVID-19	61	0.2198	0.0615	0.1702	0.2271	0.2690	-0.2295	2.1090
FT	30	0.2249	0.2713	0.0453	0.0830	0.3283	1.6936	4.9667
BMs	50	0.1632	0.0811	0.1200	0.1600	0.2400	0.0723	2.2166
SI	21	0.1531	0.0580	0.1065	0.1314	0.2188	0.5138	1.7457

We fit the UPGWD to these datasets. To substantiate its superior fitting ability, its performance is compared with that of the earlier unit Weibull distributions, including the UWD, the PUWD, the UTWD, the PUTWD, the BEWD, and the UIEWD. Furthermore, to prove the suitability of our proposed model and its superiority over these competitive models, we conduct this comparison via the following information criteria:

- The maximized log-likelihood function (log-L);
- The Akaike information criterion (AIC);
- The Bayesian information criterion (BIC);
- The Hannon–Quinn information criterion (HQIC);
- The Anderson–Darling (A-D) goodness of fit test and its *p*-value;
- The Kolmogorov–Smirnov (K-S) goodness of fit test and its *p*-value.

In general, the best fitting model is the model with the smallest values of these information criteria and the largest K-S *p*-value [47,48]. All comparison calculations and their statistical analysis were performed utilizing Algorithm 2.

Algorithm 2: Steps for the real data analysis.

1. **Step 1:** Load the dataset.
2. **Step 2:** Compute the mean, standard deviation, the three quartiles, coefficient of skewness, and coefficient of kurtosis.
3. **Step 3:** Define the PDF and CDF of each distribution.
4. **Step 4:** Estimate the parameters for each distribution using MLE and apply the function fminsearch to get the MLEs of the parameters with an initial value of [1, 1, 1] and compute the related standard errors (SE).
5. **Step 5:** Compute the log-L value.
6. **Step 6:** Create the hypothesized CDF matrix and the empirical CDF.
7. **Step 7:** Perform the K-S test and compute the K-S statistic and its *p*-value.
$$KS_{stat} = sup_v[F_n(v) - F(v)], \text{ where } F_n(v) \text{ is the empirical CDF.}$$
8. **Step 8:** Perform the A-D test and compute the A-D statistics.
$$AD_{stat} = -n - \sum_{i=1}^{n} \frac{(2i-1)}{n}\left[ln\, F(v_i) + ln\left(1 - F(v_{n+1-i})\right)\right],$$
where $F(v_i)$ is the hypothesized CDF.
9. **Step 9:** Compute the AIC, BIC, and HQIC as follows:
$$AIC = 2k - 2logL,$$
$$BIC = klog(n) - 2logL,$$
$$HQIC = 2klog\left(log(n)\right) - 2logL,$$
where k is the number of parameters.
10. **Step 10:** Display the results in a table.
11. **Step 11:** Plot the fitted histograms for each dataset.

The MLEs and their related standard errors (SEs) for the four datasets are shown in Tables A1–A4 in the Appendix. Tables 12–15 display the results of the information criteria and goodness-of-fit tests for the UPGWD against the competitive models. As can be seen from these tables, it provides the most adequate fit to all datasets, outperforming the other distributions in terms of the highest K-S *p*-value and the smallest value of the information criteria. This finding is verified by the fitted histogram shown in Figure 9.

Table 12. Goodness-of-fit results for the COVID-19 dataset.

Distribution	Log-L	AIC	BIC	CAIC	HQIC	A-D	*p*-value	K-S	*p*-value
UPGW	**86.6152**	**-167.2303**	**-160.8977**	**-157.8977**	**-164.7485**	**0.2650**	**0.3444**	**0.0709**	**0.8979**
PUW	79.4182	-152.8363	-146.5037	-143.5037	-150.3545	1.3001	-0.0079	0.1192	0.3257
PUTW	85.0720	-164.1440	-157.8114	-154.8114	-161.6622	0.4909	0.2032	0.0873	0.7085
UTW	80.9013	-157.8026	-153.5809	-151.5809	-156.1481	1.1076	0.0087	0.1177	0.3394
UW	77.1026	-150.2051	-145.9834	-143.9834	-148.5506	1.7629	-0.0478	0.1502	0.1150
UIEW	85.1622	-164.3243	-157.9917	-154.9917	-161.8425	0.3586	0.2859	0.0788	0.8150
BEW	85.0910	-164.1820	-157.8494	-154.8494	-161.7002	0.4864	0.2060	0.0865	0.7185

Table 13. Goodness-of-fit results for the FT dataset.

Distribution	Log-L	AIC	BIC	CAIC	HQIC	A-D	*p*-value	K-S	*p*-value
UPGW	**17.4621**	**-28.9242**	**-24.7206**	**-21.7206**	**-27.5795**	**0.6738**	**0.0932**	**0.1499**	**0.4660**
PUW	16.5161	-27.0321	-22.8285	-19.8285	-25.6873	0.7484	0.0647	0.1523	0.4459
PUTW	16.5353	-27.0706	-22.8670	-19.8670	-25.7258	0.7422	0.0671	0.1579	0.4010
UTW	15.1795	-26.3590	-23.5566	-21.5566	-25.4625	1.5189	-0.0268	0.2225	0.0872
UW	15.1923	-26.3847	-23.5823	-21.5823	-25.4882	1.0115	0.0169	0.1741	0.2881
UIEW	12.9043	-19.8085	-15.6049	-12.6049	-18.4638	1.4606	-0.0218	0.1941	0.1827
BEW	13.5389	-21.0778	-16.8742	-13.8742	-19.7331	1.4480	-0.0207	0.1879	0.2118

Table 14. Goodness-of-fit results for the BMs dataset.

Distribution	Log-L	AIC	BIC	CAIC	HQIC	A-D	p-value	K-S	p-value
UPGW	**57.4400**	**-108.8799**	**-103.1439**	**-100.1439**	**-106.6956**	**0.4325**	**0.2397**	**0.0909**	**0.7690**
PUW	51.5165	-97.0331	-91.2970	-88.2970	-94.8487	1.2455	-0.0032	0.1504	0.1877
PUTW	56.0497	-106.0995	-100.3634	-97.3634	-103.9151	0.6776	0.0918	0.1109	0.5334
UTW	54.9507	-105.9014	-102.0773	-100.0773	-104.4452	0.6739	0.0932	0.1183	0.4518
UW	48.6626	-93.3252	-89.5012	-87.5012	-91.8690	1.8124	-0.0521	0.1819	0.0640
UIEW	56.9979	-107.9959	-102.2598	-99.2598	-105.8116	0.4513	0.2279	0.0939	0.7351
BEW	56.0687	-106.1374	-100.4013	-97.4013	-103.9530	0.6776	0.0917	0.1103	0.5410

Table 15. Goodness-of-fit results for the SI dataset.

Distribution	Log-L	AIC	BIC	CAIC	HQIC	A-D	*p*-value	K-S	*p*-value
UPGW	**32.8851**	**-59.7701**	**-56.6366**	**-53.6366**	**-59.0901**	**0.4008**	**0.2595**	**0.1477**	**0.6953**
PUW	32.6417	-59.2834	-56.1498	-53.1498	-58.6033	0.5149	0.1882	0.1592	0.6057
PUTW	31.0817	-56.1634	-53.0298	-50.0298	-55.4833	0.9001	0.0284	0.1669	0.5471
UTW	31.5222	-59.0444	-55.4554	-53.4554	-58.8911	0.7829	0.0516	0.1709	0.5172
UW	31.6412	-59.2824	-55.6350	-53.5934	-58.8291	0.5170	0.1868	0.1592	0.6057
UIEW	32.4601	-58.9202	-55.7866	-52.7866	-58.2401	0.6302	0.1161	0.1625	0.5805
BEW	31.0842	-56.1684	-53.0348	-50.0348	-55.4883	0.9066	0.0272	0.1673	0.5442

Furthermore, we include further discussion for the theoretical comprehension of the UPGWD. This should lead researchers to apply it in their work when fitting their data compared with the PGWD. The transformation $v = exp(-t)$ in the UPGWD emphasizes the details of the data at small values of t. This scheme is significant in epidemiology, where the initial contagion data are vital for forecasting and the application of social mitigation measures. Therefore, we compared the UPGWD with its parent model, the PGWD, in fitting the COVID-19 mortality rates.

According to the goodness-of-fit results, the UPGWD appears to fit the data better than the PGWD, showing a higher log-likelihood and lower information criteria, as shown in Table 16. Figure 10 demonstrates that the UPGWD seems to fit the data more closely, especially in the lower and middle ranges of the data. The quantile–quantile (Q-Q) plots in Figure 11 show how the theoretical quantiles for the UPGWD match the empirical quantiles better than the PGWD. The empirical visualization of the CDF in Figure 12 also confirms that our model provides a better fit overall.

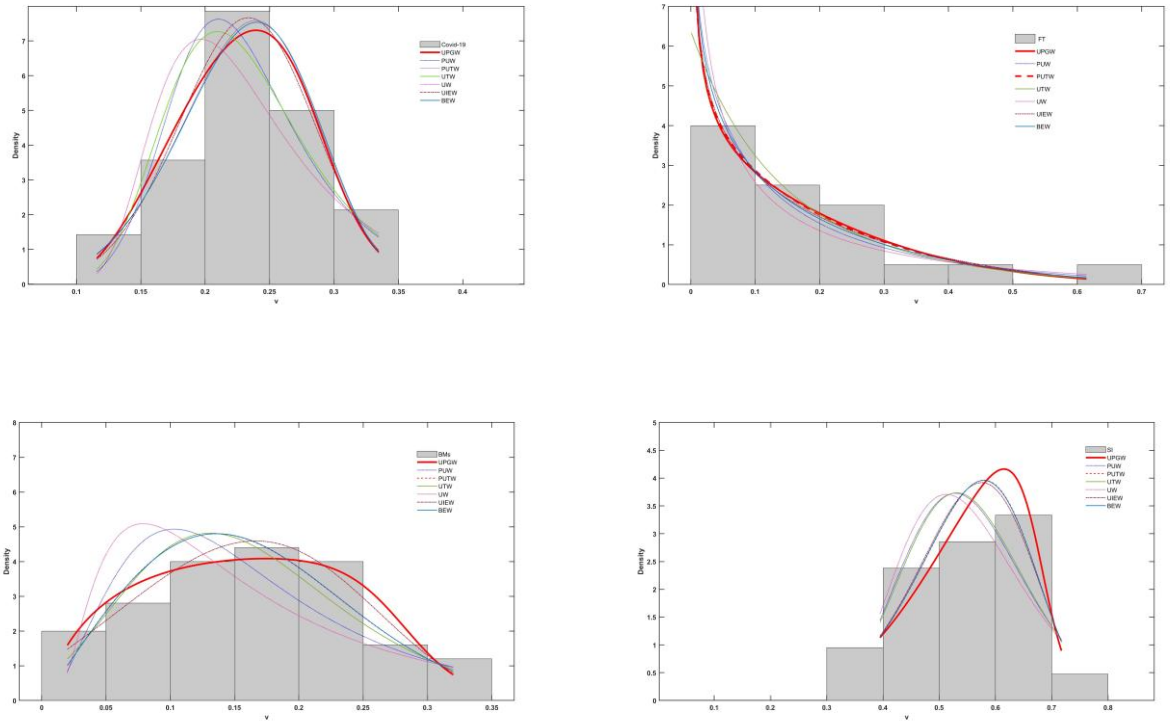

Figure 9. The fitted PDFs of the UPGWD against its competitors for the datasets.

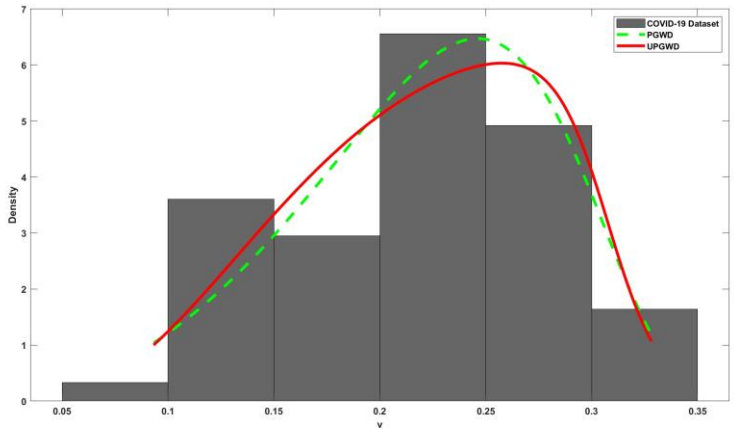

Figure 10. The fitted histogram of the UPGWD against the PGWD for the COVID-19 dataset.

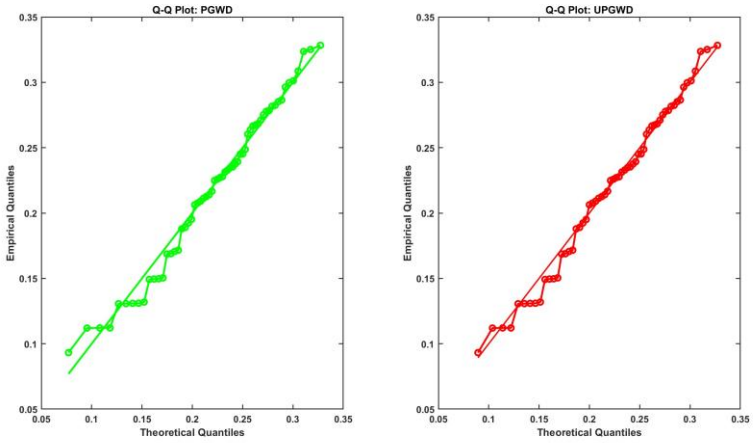

Figure 11. The Q-Q plots of the UPGWD versus the PGWD for the COVID-19 dataset.

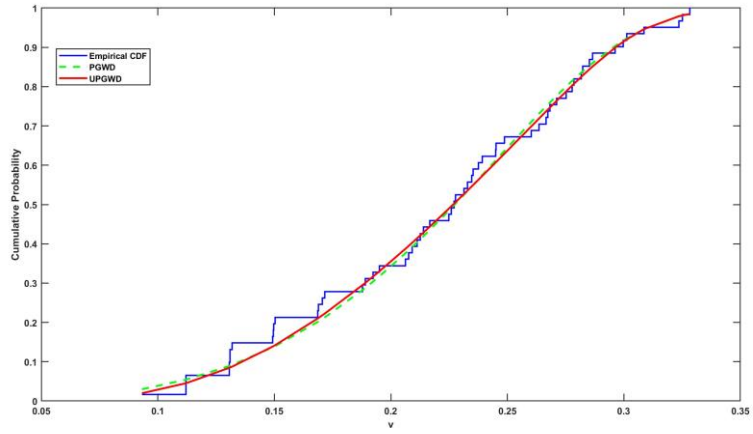

Figure 12. The empirical CDF of the UPGWD versus the PGWD for the COVID-19 dataset.

Table 16. Goodness-of-fit results of the UPGWD versus the PGWD for the COVID-19 dataset.

Criterion	PGWD	UPGWD
Log-likelihood	85.8942	86.6152
AIC	-165.7883	-167.2303
BIC	-159.4557	-160.8977
CAIC	-156.4557	-157.8977
HQIC	-163.3065	-164.7485
K-S (p-value)	0.0733 (0.8749)	0.0709 (0.8979)
A-D (p-value:)	0.3055 (0.3191)	0.2650 (0.3444)

9. Conclusions

This study proposed a novel three-parameter unit distribution called the UPGWD by applying the inverse exponential function transformation to the PGWD. We discussed its primary functions, such as its SF, HRF, and reversed HRF. Some of its statistical properties, such as moments, order statistics, its corresponding QF, and inequality measures, have been studied. In addition, some reliability measures, including the SSR coefficient, odds ratio, and Mills ratio, have been analyzed. Furthermore, we applied the MLE to estimate its parameters, and it is an efficient estimation, as verified by the MCS study. Finally, we introduced a robust witness to the superiority of our proposed model in fitting and modeling different data types from different domains by presenting four real-world datasets related to COVID-19, reliability, engineering, and radiation. The proposed UPGWD showed an adequate fit compared with other earlier unit Weibull distributions. The results of the application demonstrate that this novel distribution will be an optimal model for modeling real-world data with the unit-bounded domain. These results underscore the versatility of the UPGWD for applications related to COVID-19 mortality rates, reliability, engineering, and radiation, offering a robust three-parameter model that handles diverse, skewed datasets. Furthermore, compared with the PGWD, the transformation $v = exp(-t)$ in the UPGWD emphasizes the importance of our proposed model in epidemiology, where the initial contagion data are important for forecasting and application of social mitigation measures. Overall, the current paper contributes to extending the literature of the probability distribution theory by generating a novel unit distribution that may be an alternative to some well-known unit distributions. Moreover, in future studies, we will discuss some new facts about our proposed model and explore other estimation methods regarding its parameters with application to other datasets belonging to other real-world fields.

Author contributions

Hassan Eid Elghaly, Mohamed A. Abd Elgawad, and Boping Tian: Conceptualization, methodology, software, formal analysis, visualization, data curation, writing—original draft, preparation writing—review, and editing. Mohamed A. Abd Elgawad: Funding acquisition. Boping Tian: Validation, and supervision. All authors have read and agreed to the published version of the manuscript.

Use of Generative AI tools declaration

The authors declare they have not used artificial intelligence (AI) tools in the creation of this article.

Acknowledgments

This work was supported and funded by the Deanship of Scientific Research at Imam Mohammad Ibn Saud Islamic University (IMSIU) (grant number IMSIU-DDRSP2501).

Funding

This work was supported and funded by the Deanship of Scientific Research at Imam Mohammad Ibn Saud Islamic University (IMSIU) (grant number IMSIU-DDRSP2501).

Conflict of interest

The authors declare no conflicts of interest.

Appendix

The datasets used for the real-world data analysis in Section 8 are provided below.

Table A1. The first dataset: 61 days of COVID-19 mortality rates in the Kingdom of Saudi Arabia.

0.3086	0.3283	0.2865	0.245	0.2852	0.3251	0.2636	0.3236	0.2824	0.2817
0.3012	0.2603	0.2997	0.2393	0.2785	0.2778	0.2375	0.2963	0.2167	0.2752
0.2353	0.2347	0.1951	0.214	0.2329	0.2711	0.2126	0.2314	0.1924	0.2113
0.2683	0.2487	0.2674	0.1716	0.2666	0.2091	0.2278	0.1706	0.2271	0.189
0.2077	0.2452	0.1319	0.2259	0.1504	0.1879	0.1689	0.2063	0.2249	0.1686
0.131	0.1497	0.1309	0.1495	0.1121	0.1121	0.1307	0.112	0.1306	0.1492
0.0932									

Table A2. The second dataset: The failure times (FT) of an airplane's air-cooling system (in hours).

23	261	87	7	120	14	62	47	225	71
246	21	42	20	5	12	120	11	3	14
71	11	14	11	16	90	1	16	52	95

Table A3. The third dataset: 50 observations on burr measurements on iron sheets (in millimeters).

0.06	0.12	0.14	0.04	0.14	0.16	0.08	0.26	0.32	0.22
0.16	0.12	0.24	0.06	0.02	0.18	0.22	0.14	0.22	0.16
0.12	0.24	0.06	0.02	0.18	0.22	0.14	0.02	0.18	0.22
0.14	0.06	0.04	0.14	0.22	0.14	0.06	0.04	0.16	0.24
0.16	0.32	0.18	0.24	0.22	0.04	0.14	0.26	0.18	0.16

Table A4. The fourth dataset: 21 values of SI for both irradiated and unirradiated peppermint packages.

2.463871049	2.534601047	2.342430823	2.120520465	2.235678759
2.177037749	1.791202270	1.865753707	1.754017205	1.498275501
1.411231151	2.183200002	2.252259207	1.394837635	2.029383778
2.287564493	2.096705442	1.970275512	1.526788015	1.426894443
1.452740448				

Table A5. MLEs and SEs for the COVID-19 dataset.

Distribution	$\hat{\alpha}$	SE$(\hat{\alpha})$	$\hat{\beta}$	SE $(\hat{\beta})$	$\hat{\lambda}$	SE $(\hat{\lambda})$
UPGW	28.4478	13.1832	0.0799	0.0415	0.0096	0.0162
PUW	0.0175	0.0101	6.2031	0.5901	-2.6956	1.3586
PUTW	4.1966	0.4335	1.3274	0.7603	-287.3688	0.0000
UTW	-	-	13.5677	1.3127	17.7482	4.7201
UW	0.0670	0.0218	5.1549	0.4838	-	-
UIEW	5.1699	2.4305	1.3955	1.1859	7.3684	1.8811
BEW	373.8948	110.8579	430.0058	30.4274	0.0097	0.0009

Table A6. MLEs and SEs for the FT dataset.

Distribution	$\hat{\alpha}$	SE$(\hat{\alpha})$	$\hat{\beta}$	SE $(\hat{\beta})$	$\hat{\lambda}$	SE $(\hat{\lambda})$
UPGW	1.1351	0.1757	55.5166	76.7913	0.0044	0.0061
PUW	0.6369	0.2948	1.1297	0.2606	2.4610	1.4795
PUTW	0.7535	0.1421	0.7772	0.3845	-3.6222	1.6957
UTW	-	-	1.0520	0.3667	-3.9952	1.3742
UW	0.2786	0.0858	1.4562	0.2262	-	-
UIEW	0.0983	0.0141	453795.8054	273.9724	14.1360	0.2799
BEW	1.3837	0.3362	0.9395	0.0000	0.5802	0.0000

Table A7. MLEs and SEs for the BMs dataset.

Distribution	$\hat{\alpha}$	SE$(\hat{\alpha})$	$\hat{\beta}$	SE $(\hat{\beta})$	$\hat{\lambda}$	SE $(\hat{\lambda})$
UPGW	14.9382	6.4304	0.0956	0.0467	0.0332	0.0390
PUW	0.0184	0.0103	3.7890	0.3871	-3.3696	1.4948
PUTW	2.0752	0.2544	0.1038	0.0427	-318.8584	0.0000
UTW	-	-	11.2875	1.3854	4.4443	1.0476
UW	0.0876	0.0288	3.0519	0.3081	-	-
UIEW	3.0965	1.4029	1.5016	1.2589	6.2890	1.2816
BEW	33.1375	13.9032	0.2154	0.0000	9.6440	0.0000

Table A8. MLEs and SEs for the SI dataset.

Distribution	$\widehat{\alpha}$	SE$(\widehat{\alpha})$	$\widehat{\beta}$	SE $(\widehat{\beta})$	$\hat{\lambda}$	SE $(\hat{\lambda})$
UPGW	4.9292	0.0000	12.2554	0.0000	0.0014	0.0000
PUW	0.0096	0.0161	6.3019	1.6197	0.0573	1.9105
PUTW	2.9498	0.4999	1.7903	1.8152	-100.3155	58.0506
UTW	-	-	19.4615	3.5558	14.3203	6.7314
UW	0.0093	0.0086	6.3368	1.1198	-	-
UIEW	0.7488	0.1238	2700.2284	174.9647	13.6332	1.3301
BEW	175.1918	127.8874	0.0198	0.0121	148.3859	83.4648

References

1. M. Muhammad, B. Abba, J. Xiao, N. Alsadat, F. Jamal, M. Elgarhy, A new three-parameter flexible unit distribution and its quantile regression model, *IEEE Access*, **12** (2024), 156235–156251. https://doi.org/10.1109/ACCESS.2024.3485219
2. A. Fayomi, A. S. Hassan, H. Baaqeel, E. M. Almetwally, Bayesian inference and data analysis of the unit–power Burr X distribution, *Axioms*, **12** (2023), 297. https://doi.org/10.3390/axioms12030297
3. P. Kumaraswamy, A generalized probability density function for double-bounded random processes, *J. Hydrol.*, **46** (1980), 79–88. https://doi.org/10.1016/0022-1694(80)90036-0
4. I. E. Okorie, E. Afuecheta, H. S. Bakouch, Unit upper truncated Weibull distribution with extension to 0 and 1 inflated model – theory and applications, *Heliyon*, **9** (2023), e22260. https://doi.org/10.1016/j.heliyon.2023.e22260
5. S. Bashir, B. Masood, L. A. Al-Essa, A. Sanaullah, I. Saleem, Properties, quantile regression, and application of bounded exponentiated Weibull distribution to Covid-19 data of mortality and survival rates, *Sci. Rep.*, **14** (2024), 14353. https://doi.org/10.1038/s41598-024-65057-6
6. P. L. Gupta, R. C. Gupta, The monotonicity of the reliability measures of the beta distribution, *J. Appl. Math. Lett.*, **13** (2000), 5–9. https://doi.org/10.1016/S0893-9659(00)00025-2
7. C. W. Topp, F. C. Leone, A family of J-shaped frequency functions, *J. Am. Stat. Assoc.*, **50** (1955), 209–219. https://doi.org/10.2307/2281107
8. J. Mazucheli, A. F. B. Menezes, M. E. Ghitany, The unit-Weibull distribution and associated inference, *J. Appl. Probab. Stat.*, **13** (2018), 1–22.
9. A. A. Suleiman, H. Daud, A. I. Ishaq, M. Othman, H. M. Alshanbari, S. N. Alaziz, A novel extended Kumaraswamy distribution and its application to Covid-19 data, *Eng. Rep.*, **6** (2024), e12967. https://doi.org/10.1002/eng2.12967
10. A. Grassia, On a family of distributions with argument between 0 and 1 obtained by transformation of the gamma and derived compound distributions, *Aust. J. Stat.*, **19** (1977), 108–114. https://doi.org/10.1111/j.1467-842X.1977.tb01277.x
11. P. R. Tadikamalla, On a family of distributions obtained by the transformation of the gamma distribution, *J. Stat. Comput. Simul.*, **13** (1981), 209–214. https://doi.org/10.1080/00949658108810497
12. E. Gómez-Déniz, M. A. Sordo, E. Calderín-Ojeda, The log–Lindley distribution as an alternative to the beta regression model with applications in insurance, *Insur. Math. Econ.*, **54** (2014), 49–57. https://doi.org/10.1016/j.insmatheco.2013.10.017

13. J. Mazucheli, A. F. B. Menezes, S. Chakraborty, On the one parameter unit-Lindley distribution and its associated regression model for proportion data, *J. Appl. Stat.*, **46** (2019), 700–714. https://doi.org/10.1080/02664763.2018.1511774
14. J. Mazucheli, A. F. B. Menezes, S. Dey, The unit-Birnbaum-Saunders distribution with applications, *Chil. J. Stat.*, **9** (2018), 47–57.
15. J. Mazucheli, A. F. Menezes, S. Dey, Unit-Gompertz distribution with applications, *Statistica*, **79** (2019), 25–43. https://doi.org/10.6092/issn.1973-2201/8497
16. M. E. Ghitany, J. Mazucheli, A. F. B. Menezes, F. Alqallaf, The unit-inverse Gaussian distribution: a new alternative to two-parameter distributions on the unit interval, *Commun. Stat.-Theory Methods*, **48** (2019), 3423–3438. https://doi.org/10.1080/03610926.2018.1476717
17. A. T. Ramadan, A. H. Tolba, B. S. El-Desouky, A unit half-logistic geometric distribution and its application in insurance, *Axioms*, **11** (2022), 676. https://doi.org/10.3390/axioms11120676
18. R. A. R. Bantan, C. Chesneau, F. Jamal, M. Elgarhy, M. H. Tahir, A. Ali, et al., Some new facts about the unit-Rayleigh distribution with applications, *Mathematics*, **8** (2020), 1954. https://doi.org/10.3390/math8111954
19. I. Shah, B. Iqbal, M. F. Akram, S. Ali, S. Dey, Unit Nadarajah and Haghighi distribution: properties and applications in quality control, *Sci. Iran.*, 2021. https://doi.org/10.24200/sci.2021.57302.5167
20. F. A. Bhatti, A. Ali, G. G. Hamedani, M. Ç. Korkmaz, M. Ahmad, The unit generalized log Burr XII distribution: properties and application, *AIMS Math.*, **6** (2021), 10222–10252. https://doi.org/10.3934/math.2021592
21. M. Ç. Korkmaz, C. Chesneau, Z. S. Korkmaz, The unit folded normal distribution: a new unit probability distribution with the estimation procedures, quantile regression modeling and educational attainment applications, *J. Reliab. Stat. Stud.*, **15** (2022), 261–298. https://doi.org/10.13052/jrss0974-8024.15111
22. H. E. Elghaly, M. A. Abd Elgawad, B. Tian, A novel alternative to the beta and Kumaraswamy distributions for double bounded hydroclimatology data, *IEEE Access*, **13** (2025), 111217–111236. https://doi.org/10.1109/ACCESS.2025.3583265
23. F. Condino, F. Domma, Unit distributions: a general framework, some special cases, and the regression unit-Dagum models, *Mathematics*, **11** (2023), 2888. https://doi.org/10.3390/math11132888
24. W. Weibull, A statistical distribution function of wide applicability, *J. Appl. Mech.*, 1951, 1–5.
25. A. S. Hassan, R. S. Alharbi, Different estimation methods for the unit inverse exponentiated Weibull distribution, *Commun. Stat. Appl. Methods*, **30** (2023), 191–213. https://doi.org/10.29220/CSAM.2023.30.2.191
26. A. M. A. El-latif, O. A. Alqasem, J. K. Okutu, C. Tanış, L. P. Sapkota, N. A. Noori, A flexible extension of the unit upper truncated Weibull distribution: statistical analysis with applications on geology, engineering, and radiation data, *J. Radiat. Res. Appl. Sci.*, **18** (2025), 101434. https://doi.org/10.1016/j.jrras.2025.101434
27. T. Dimitrakopoulou, K. Adamidis, S. Loukas, A lifetime distribution with an upside-down bathtub-shaped hazard function, *IEEE Trans. Reliab.*, **56** (2007), 308–311. https://doi.org/10.1109/TR.2007.895304
28. G. Azedine, Characterization of the power distribution based on the lower records, *Appl. Math. Sci.*, **7** (2013), 5259–5267. https://doi.org/10.12988/ams.2013.36326

29. M. H. Tahir, M. Alizadeh, M. Mansoor, G. M. Cordeiro, M. Zubair, The Weibull-power function distribution with applications, *Hacet. J. Math. Stat.*, **45** (2016), 245–265.
30. A. Mohammadi, M. Jalili-Ghazizadeh, I. Moslehi, E. Yousefi-Khoshqalb, Survival analysis of water distribution network under intermittent water supply conditions, *Water Supply*, **20** (2020), 3531–3541. https://doi.org/10.2166/ws.2020.228
31. K. Edward, K. Beata, K. Dariusz, M. Dariusz, Survival function in the analysis of the factors influencing the reliability of water wells operation, *Water Resour. Manage.*, **33** (2019), 4909–4921. https://doi.org/10.1007/s11269-019-02419-0
32. E. J. Veres-Ferrer, J. M. Pavía, On the relationship between the reversed hazard rate and elasticity, *Stat. Pap.*, **55** (2014), 275–284. https://doi.org/10.1007/s00362-012-0470-1
33. A. S. Hassan, A. Al-Omari, H. F. Nagy, Stress–strength reliability for the generalized inverted exponential distribution using MRSS, *Iran. J. Sci. Technol. Trans. A: Sci.*, **45** (2021), 641–659. https://doi.org/10.1007/s40995-020-01033-9
34. A. J. Lemonte, A new exponential-type distribution with constant, decreasing, increasing, upside-down bathtub and bathtub-shaped failure rate function, *Comput. Stat. Data Anal.*, **62** (2013), 149–170. https://doi.org/10.1016/j.csda.2013.01.011
35. M. R. Spiegel, S. Lipschutz, J. Liu, *Mathematical handbook of formulas and tables*, 3 Eds., New York: McGraw-Hill, 2009.
36. F. W. J. Olver, D. W. Lozier, R. F. Boisvert, C. W. Clark, The *NIST handbook of mathematical functions*, New York: Cambridge University Press, 2010.
37. S. Ferrari, F. Cribari-Neto, Beta regression for modelling rates and proportions, *J. Appl. Stat.*, **31** (2004), 799–815. https://doi.org/10.1080/0266476042000214501
38. A. L. Bowley, *Elements of statistics*, 1926.
39. J. J. A. Moors, A quantile alternative for kurtosis, *J. R. Stat. Soc. Ser. D (Stat.)*, **37** (1988), 25–32. https://doi.org/10.2307/2348376
40. G. M. Mansour, M. A. Abd Elgawad, A. S. Al-Moisheer, H. M. Barakat, M. A. Alawady, I. A. Husseiny, et al., Bivariate Epanechnikov-Weibull distribution based on Sarmanov copula: properties, simulation, and uncertainty measures with applications, *AIMS Math.*, **10** (2025), 12689–12725. https://doi.org/10.3934/math.2025572
41. T. Makelainen, K. Schmidt, G. P. H. Styan, On the existence and uniqueness of the maximum likelihood estimate of a vector-valued parameter in fixed-size samples, *Ann. Statist.*, **9** (1981), 758–767. https://doi.org/10.1214/aos/1176345516
42. Z. Shah, D. M. Khan, S. Hussain, N. Iqbal, J. T. Seong, S. N. Alaziz, et al., A new flexible exponent power family of distributions with biomedical data analysis, *Heliyon*, **10** (2024), e32203. https://doi.org/10.1016/j.heliyon.2024.e32203
43. O. A. Alamri, A. H. Alessa, E. Hussam, M. H. Alhelali, M. Kilai, Statistical modelling for the Covid-19 mortality rate in the kingdom of Saudi Arabia, *Alex. Eng. J.*, **68** (2023), 517–526. https://doi.org/10.1016/j.aej.2023.01.024
44. H. Linhart, W. Zucchini, *Model selection*, John Wiley & Sons, 1986.
45. R. Dasgupta, On the distribution of Burr with applications, *Sankhya B*, **73** (2011), 1–19. https://doi.org/10.1007/s13571-011-0015-y
46. N. A. H. Abdelfattah, R. M. Sayed, Comparative efficacy of gamma and microwave radiation in protecting peppermint from infestation by drugstore beetle (Stegobium paniceum) L., *Int. J. Trop. Insect Sci.*, **42** (2022), 1367–1372. https://doi.org/10.1007/s42690-021-00655-9

47. M. Muhammad, L. Liu, A new three parameter lifetime model: the complementary Poisson generalized half logistic distribution, *IEEE Access*, **9** (2021), 60089–60107. https://doi.org/10.1109/ACCESS.2021.3071555
48. E. E. Hassan, D. Zhang, The usage of logistic regression and artificial neural networks for evaluation and predicting property-liability insurers' solvency in Egypt, *Data Sci. Finance Econ.*, **1** (2021), 215–234. https://doi.org/10.3934/DSFE.2021012

AIMS Press